The Paton WELDING JOURNAL

June 2000 # 6

English translation of the monthly «Avtomaticheskaya Svarka» journal published in Russian since 1948

«The Paton Welding Journal» monthly is published by the E.O. Paton Electric Welding Institute of the National Academy of Sciences of Ukraine with the support rendered by the International Association «Welding».

Promotion group:
V.N.Lipodaev, V.I.Lokteva
A.T.Zelnichenko (Exec. director)
Translators:
S.A.Fomina, I.N.Kutianova, T.K.Vasilenko
Editorial and advertising offices are located at PWI, Dept. 51, 11, Bozhenko str., 03680, Kyiv, Ukraine.
Tel.: (38044) 227 67 57
Fax: (38044) 268 04 86
E-mail: paton@i.kiev.ua

Subscriptions:
$460, 12 issues

«The Paton Welding Journal» Website:
http://www.nas.gov.ua/pwj

CONTENTS

STRESS CONCENTRATION IN THE AREAS OF CORROSION DAMAGE OF PIPELINES

E.F. GARF[1], M.A. NETREBSKIY[1], P.S. YUKHIMETS[1] and S.V. KOBELSKIY[2]
[1]The E.O. Paton Electric Welding Institute, NASU, Kyiv, Ukraine
[2]Institute of Problems of Strength, NASU, Kyiv, Ukraine

ABSTRACT

Finite element method and electric stain measurement means were used to study the concentration of stresses in the zone of corrosion damage of pipelines, simulated by the surface of an ellipsoid and a cylinder. It is shown that these defects can create a risk of cyclic elasto-plastic fracture while the required level of static strength is ensured. An approximate dependence for determination of stress concentration in the zone of surface corrosion damage has been determined more precisely.

Key words: *pipelines, surface defects, finite element method, stress concentration.*

A characteristic feature of various purpose pipelines is development during their operation of defects of an arbitrary shape with a small area of pipe damage. Experience of gas and oil pipeline operation points to the possibility of appearance of a large number of defects of corrosion origin on the outer surface. In the case of NPP piping and inner station piping of TPP, the defects resulting from the erosion-corrosion processes, are located on the inner surface.

Irrespective of the pipeline purpose, causes for development and location of a defect, in the case of its detection, the personnel responsible for safe service of the pipeline, is faced with the problem of determination of the residual life.

A semi-empirical procedure of pipe strength determination [1] became widely accepted now, which is based on numerous theoretical and experimental studies of the pipeline static strength and depends on the ratio of geometrical parameters of the pipeline and the defect.

The NPP and TPP pipelines are exposed to cyclic loads in service, as a result of which they can reach the limit state in the defect zone in terms of strength under repeated-static loading.

Forecasting of the residual life of the pipeline under cyclic loading is based, besides the operational load and cyclic properties of the material, on the data of its stressed-strained state (SSS), primarily in the stress concentration zones. The results of the design and experimental investigations given below, are a development of such an approach in relation to surface defects of pipelines.

The main tool used to study SSS in the damage zone was the PIPE software package developed in the Institute of Problems of Strength, which is part of SPACE package [2] for determination by the finite element method (FEM) of the three-dimensional thermal and SSS of structures. The specialised PIPE package is to be used for design of pipeline system elements (equivalent and non-equivalent cross-section cylindrical and conical T-joints, branch-pipes, defective pipes) under the impact of internal pressure, bending moments, torques and temperature fields.

The geometrical model of each of the objects included into the package library, was constructed in the parametral form. In order to go over from this model to the real model it is necessary to assign the value of a number of the characteristic parameters (dimensions) of the object.

In the majority of practical cases the considered defects can be rather accurately described in terms of geometry by an ellipsoid. Proceeding from that, a series of computations were performed for a pipe with one or several defects on the outer or inner surface with different ratios of the ellipsoid axes lengths (Figure 1, *a, b*).

Figure 2 shows the circumferential σ_φ and axial σ_z stresses and intensity σ_i of stresses on the inner and outer surfaces of a pipe of 322 mm diameter with 7 mm wall thickness, when the defect (length c = 25 mm, depth b = 1.4 mm, width d = 35 mm) is located on its inner surface, as well as the stress intensity when the defect is located on the outside. Stress distribution at unit internal pressure is given along φ and z directions which coincide with the ellipsoid axes of symmetry.

As we can see (Figure 2, *a*, curves *1* – *3*), the maximal stresses arise on the inner defect surface in its tip. The values of the circumferential and axial stresses are close to the principal stresses. Closer to the defect edges the stresses gradually decrease, while at its very boundary their jump-like change is possible. At a distance approximately equal to the defect length in the appropriate direction, the stresses are stabilised at the level of nominal

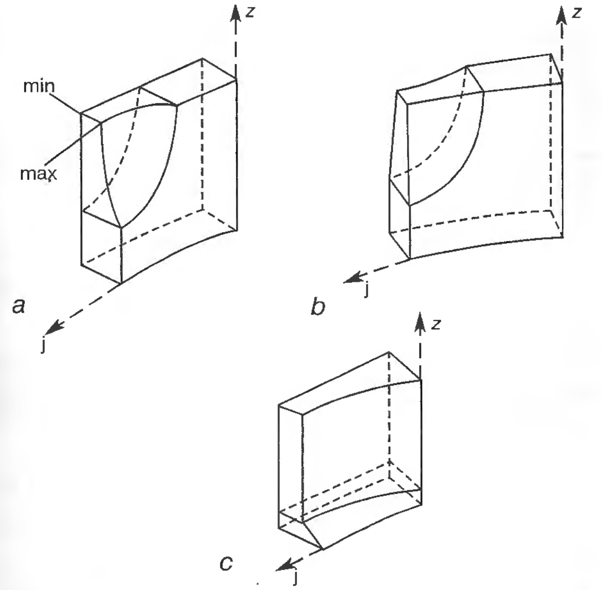

Figure 1. Models of defects used in FEM computation: *a, b* — ellipsoid on the inner and outer surface, respectively; *c* — cylinder on the inner surface

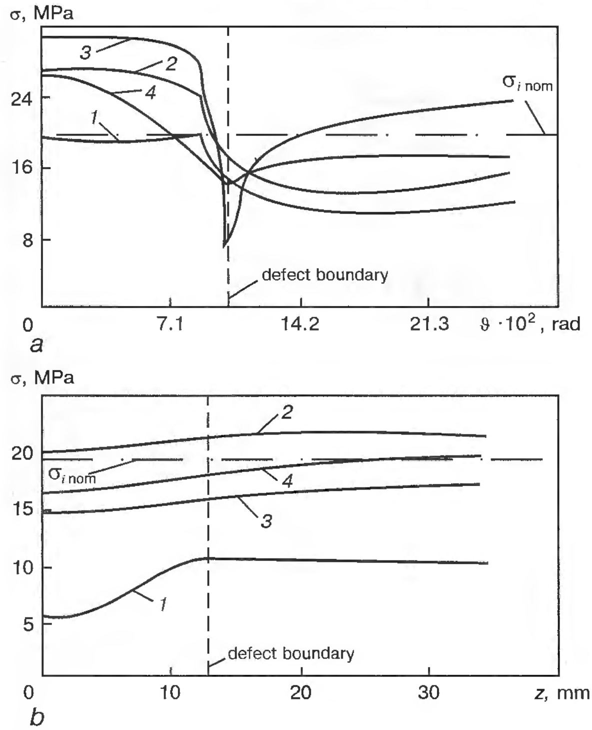

Figure 2. Comparison of stresses on the surfaces of defects (*a*) and on the surfaces opposite to them (*b*): *1* — σ_z; *2* — σ_i; *3* — σ_φ (defect on the pipe inner surface); *4* — σ_i (defect on the pipe outer surface); ϑ, *z* — central angle and distance measured from the defect middle, respectively

values. The ratios $\sigma_{\varphi\ max}/\sigma_{\varphi\ nom} \approx 1.4$; $\sigma_{z\ max}/\sigma_{z\ nom} \approx 1.7$. The stresses along the other axis of symmetry are distributed similarly.

In the point opposite to the defect on the pipe outer surface (Figure 2, *b*, curves *1 – 3*), the stresses are minimal. Gradual increase and equalising of stresses on the level of the nominal values occurs closer the edges. Note that such a ratio of stresses on the pipe inner and outer surface, is characteristic of bending. Ratios $\sigma_{\varphi\ min}/\sigma_{\varphi\ nom} \approx$ ≈ 0.7; $\sigma_{z\ min}/\sigma_{z\ nom} \approx 0.45$. The stresses in φ direction are distributed similarly. The coefficients of stress concentration calculated proceeding from the extreme values of stress intensity (allowing for the bulk stressed state) are

$$\alpha_{max} = \frac{\sigma_{i\ max}}{\sigma_{i\ nom}} = 1.38,$$

on the defect surface (Figure 1, *a*, max point) and

$$\alpha_{min} = \frac{\sigma_{i\ min}}{\sigma_{i\ nom}} = 0.72.$$

on the pipe outer surface (Figure 1, *a*, min point).

As shown by the data derived when the same dimensions of the ellipsoid were used in calculations, the nature of stresses distribution over the defect surface and the surface opposite to it does not depend on whether the defect is located on the outer or the inner surface of the pipe (Figure 2, *a*, curves *2, 4*; Figure 2, *b*, curves *2, 4*). With the defect located on the outside, the decrease of stresses on its surface is more abrupt. Therefore, although the maximal values of stress intensity on the surfaces of the inner and outer defects do not essentially differ in such a case, their values averaged by length or width are higher in the case of an internal defect.

On the whole, with some differences in the components of the stress tensor, stress concentration on the surfaces of the inner and outer defects is practically the same.

The issue of the defects interaction with SSS was studied based on comparison of the results of computation of one defect and four defects equal to it, located symmetrically around the perimeter of the pipe inner surface (Figure 3). In the case of four defects, an increase of stresses by ≈ 20 % was found.

The validity of the derived results was verified in experimental investigation of SSS. An experimental sample consisted of a piece of St.20 pipe of 322 mm diameter with 7 mm wall thickness, and 615 mm length. Local wall thinning, namely defects, were made on the pipe inner and outer sur-

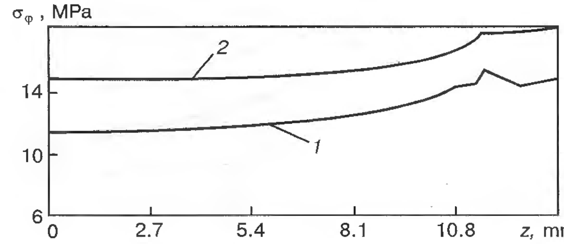

Figure 3. Influence of the number of defects on circumferential stress σ_φ in a pipe of 322 mm diameter with 7 mm wall thickness: *1* — one defect; *2* — four symmetrically located defects

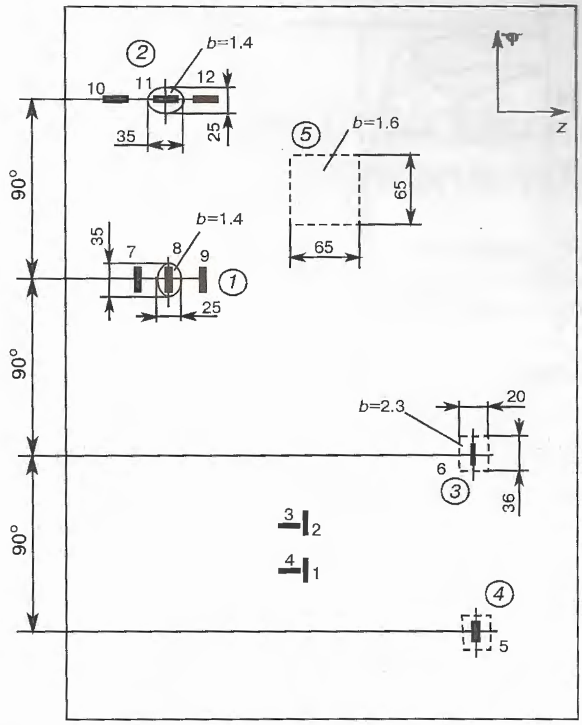

Figure 4. Schematic of defects (numbers in circles) and strain gauges (*1 – 12*) location on the development of the sample cylindrical surface. Dashed line indicates defects on the sample inner surface

faces (Figure 4). The geometrical dimensions of the defects were assigned so that the static strength of the pipe by the conditions of study [1] were not decreased. The defects marked by numbers *3, 4* were introduced with a cylindrical mill (see Figure 1, *c*) and had the same dimensions. Defects *1, 2* on the outer surface, made with a hand grinder, were shaped as part of an ellipsoid and were actually a modification of one defect turned through 90°. Defect *5* was located on the inner surface and was not an object of investigation.

After welding on the plugs and mounting strain gauges KF-5 with 10 mm gauge length on the outer surface (Figure 4), the sample was loaded by inner pressure up to 10 MPa. The pressure was raised stepwise, with 2 MPa interval. Strains were measured at each loading level. Readings of sensors *1 – 4* were used for monitoring the strain gauges accuracy. The difference between the design stresses

$$\sigma_\varphi = \frac{P(D_n - h)}{2h}, \tag{1}$$

$$\sigma_z = \frac{P(D_n - h)}{4h} \tag{2}$$

(where P is the inner pressure, MPa; D_n is the outer diameter; h is the wall thickness) and their experimental values

$$\sigma_\varphi = \frac{E}{1-\mu^2}(\varepsilon_\varphi + \mu\,\varepsilon_z), \tag{3}$$

$$\sigma_z = \frac{E}{1-\mu^2}(\varepsilon_z + \mu\,\varepsilon_\varphi) \tag{4}$$

(where $E = 2.1\cdot10^5$ MPa is the material modulus of elasticity; $\mu = 0.3$ is the Poisson's ratio; ε_φ and ε_z are the relative axial and circumferential strains, respectively) was equal to $\Delta\sigma_\varphi = 1.6$ %; $\Delta\sigma_z = 1.8$ %.

The results of comparison of experimental strains with FEM design values are given in Table 1. The design strain values averaged by the sensor gauge length (10 mm) are used in the Table.

A certain stable excess of the experimental strain values over the design is, probably, attributable to the fact that SSS analysis did not allow for the influence of the defect interaction. On the other hand, a rather close correlation of the performed computations with the experimental results permitted assessment of the dependence used in engineering practice for evaluation of SSS in the corrosion damage zone [3]:

$$a_\sigma = 1 + \frac{2\dfrac{b}{d}\left[1.12 - 0.48\dfrac{b}{c} + 0.13\dfrac{b}{c}\left(3\dfrac{b}{c} - 2\dfrac{b}{h}\right)\right]}{1 - \dfrac{b}{h}\left(1 - 0.75\dfrac{b}{c}\right)} \times \tag{5}$$

$$\times\sqrt{1 + \frac{5\pi\lambda^2}{32}},$$

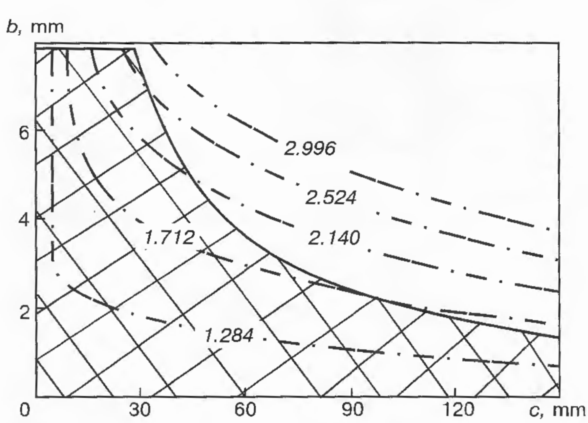

Figure 5. Stress concentration depending on the defect length and depth (full curve shows limit admissible dimensions [3], admissible defect area is hatched)

Table 1

Sensor No.	Experiment $\varepsilon\cdot10^{-5}$	FEM design $\varepsilon\cdot10^{-5}$	Error, %
8	1.305	1.115	14.6
5, 6	0.663	0.655	1.2
11	0.447	0.419	6.3
12, 14	0.185	0.180	2.7

Table 2

D_n, mm	h, mm	c, mm	b, mm	d, mm	Surface	a^*	a^{**}	a^*/a^{**}, %
325	9	38.2	3.15	19.1	Internal	1.85	2.22	83
322	7	25.0	1.40	35.0	Outer	1.15	1.37	84
322	7	25.0	2.40	25.0	»	1.21	2.13	61
322	7	20.0	2.30	26.0	Internal	1.24	1.56	79
322	7	35.0	1.40	25.0	Outer	1.25	1.42	88

*Calculated by equation (5).
**FEM.

where a_σ is the coefficient of stress concentration in the defect zone; λ is the function allowing for surface curvature and having the form of

$$\lambda^2 = \frac{c^2}{Rh}[12(1-\mu^2)]^{1/2},$$

where R is the pipe radius.

Table 2 gives the data of calculation of the coefficient of stress concentration by equation (5) and FEM.

As one can see the error in determination of the maximal active stress in the region of the damage using dependence (5) falls within the range of 10 to 40 %. In its turn, such an inaccuracy in determination of the pipeline residual life can lead to its overestimation by 30 to 300 %.

Figure 5 shows the lines of isoconcentration of stresses for a pipe of 600 mm diameter with 12 mm wall thickness at the pressure of 6.2 MPa calculated by equation (5), depending on the change of the length and depth of the defect with its fixed width (20 mm). The figure shows that the stress concentration in the region of the admissible (by static strength criteria) dimensions of the defects can reach significant values, thus creating a risk of pipeline failure as a result of the fatigue crack initiation. Corrosion pits and narrow cavities are especially dangerous.

In view of the above said, it seems rational to introduce the correction factor of 1.4 into calculation of the stress concentration by equation (5). Such a correction is the more justified since the description of the existing defect by an ellipsoid can in some cases lower the actual stress concentration. Calculation of the SSS of a cylindrical defect (see Figure 1, *c*) by FEM with the maximal closeness of the design geometry to the actual one (Figure 1, *a*) and with the defect approximation (Figure 1, *b*) by an inscribed ellipsoid, showed that the maximal stress intensities in the first case are by 13.5 % higher than in the second case.

CONCLUSIONS

1. Stress concentration in the zone of the pipeline corrosion damage can reach considerable values and create a risk of cyclic elasto-plastic fracture under the conditions of provision of static strength.

2. A satisfactory correlation of FEM computation results with the experimental data was confirmed.

3. The approximate dependence for determination of stress concentration in the zone of surface corrosion damage was determined more precisely.

REFERENCES

1. *Cases of ASME Boiler and Pressure Vessels Code.* Case No. 480.
2. (1993) Development of an information-technological system for up-to-date personal computers for investigation of three-dimensional models of thermo-plastic solids in order to determine the thermal-stressed state of elements of mechanical engineering structures at quasi-static impacts. In: *R&D report UkrINTEI*. Kyiv.
3. Fokin, M.F., Trubitsin, V.A., Nikitina, E.A. (1986) *Evaluation of service fatigue life of the main oil pipelines in the defect zone*. Moscow: VNIIOENG.

EFFECT OF NITRIDE-FORMING ELEMENTS ON COMPOSITION AND STRUCTURE OF LOW-ALLOYED WELD METAL

V.N. SHLEPAKOV, A.S. KOTELCHUK and **S.M. NAUMEIKO**
The E.O. Paton Electric Welding Institute, NASU, Kyiv, Ukraine

ABSTRACT

The effect of a complex alloying with nitride-forming elements on structure of a low-alloyed weld metal is studied. A feasibility of prediction of the primary microstructure of a single-pass weld is shown.

Key words: *arc welding, low-alloyed steel, nitrogen, nitride-forming elements, microstructure, allotriomorphous ferrite, Widmanstätten ferrite, acicular ferrite.*

Interaction of molten metal with nitrogen in welding with a self-shielding flux-cored wire is proceeding under conditions when the overheated metal of drops and pool absorbs nitrogen in the amounts capable to exceed its solubility in metal [1]. During cooling the molten metal a significant saturation of the weld pool metal with nitrogen over the whole volume can be attained due to decrease in the solubility. This can cause the pore formation [2]. The most probable pore formation is observed at the boundaries of grains of non-fused crystals, in spaces of the growing serrated front of crystals, and also on non-metallic inclusions within the molten metal volume.

The actual problem for the self-shielding welding consumables is an alloying of the weld metal with titanium or aluminium through the core of the flux-cored wire that can decrease significantly the metal susceptibility to porosity, as the titanium and aluminium bind the large amount of nitrogen into nitrides and prevent the evolution of gas bubbles [3]. The metal alloying with these nitride-forming elements as aluminium and titanium greatly influences the structure of the weld metal and its mechanical properties. This article describes the effect of a complex alloying on the structure of the weld metal which contains aluminium and titanium.

Formation of nitrides in metal solutions depending on their composition, temperature and partial pressure of nitrogen in a gas phase can be evaluated using the thermodynamic calculations. The nitride formation is preceded with a surface absorption of nitrogen and its transporting into the metal volume.

Solubility of nitrogen in the iron melt at 101.325 kPa partial pressure of nitrogen can be expressed [1] with the help of an equilibrium constant

$$\lg K_N = \lg (a_N/P_{N_2}^{0.5}) = A/T + B = -188/T - 1.25,$$

$$a_N = [N] f_N,$$

$$\lg [N] = \lg K_N - \lg f_N + 0.5 \lg P_{N_2},$$

where [N] is the nitrogen content in the molten metal; f_N is the coefficient of nitrogen activity in the melt; K_N is the constant of nitrogen equilibrium; a_N is the nitrogen activity; P_{N_2} is the partial pressure of nitrogen; A and B are the empiric coefficients.

The coefficient of nitrogen activity is calculated using parameters of nitrogen interaction with components of metal melt at temperature 1853 K:

$$\lg f_N = \sum_{i=1}^{n} e_N^i \, [i],$$

where e_N^i is the thermodynamic parameter of interaction of the first-order nitrogen; $[i]$ is the component content in the metal melt [1, 2].

$e_{[N]}^{[Al]} = -0.028$; $e_{[N]}^{[Ti]} = -0.45$.

The nitride formation occurs from the reaction [MeN] = [Me] + [N].

Aluminium effect on the nitrogen content in metal is described by the relationship

$$\lg[N] = -1.351 - e_{[N]}^{[Al]} [Al],$$

$$[N] = 10^{-1.351 + 0.028[Al]}.$$

Within the temperature interval of 1800 – 2000 K [1, 2]

$$\lg K_{AlN} = \lg[Al][N] = -10012/T + 4.04,$$

where K_{AlN} is the constant of equilibrium of aluminium nitride; [Al] and [N] are the contents of aluminium and nitrogen.

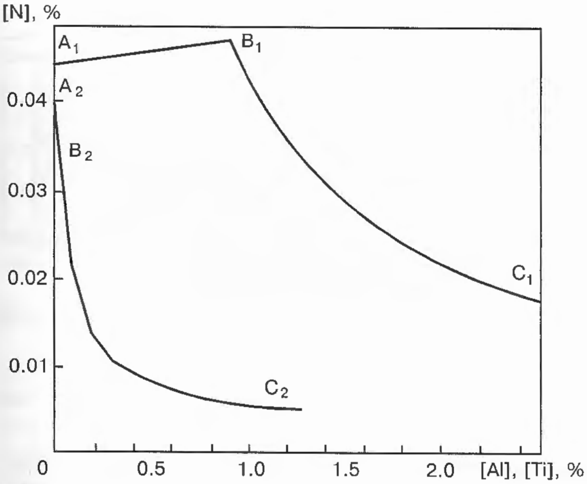

Figure 1. Diagram of nitrogen dissolution: A_1B_1, A_2B_2 — from the reaction $0.5N_{2[g]} = [N]$; B_1C_1 — from reaction $AlN = [Al] + [N]$; B_2C_2 — from reaction $TiN = [Ti] + [N]$

Then,

$$\lg [Al] + \lg [N] = -10012/T + 4.04 = -1.363,$$

$$[N] = 10^{-1.363 - \lg [Al]}.$$

Similarly, we calculate the titanium effect on nitrogen content in metal:

$$\lg [N] = -1.351 + 0.45 [Ti],$$

$$[N] = 10^{-1.351 + 0.45 [Ti]}.$$

The formation of titanium nitride can be expressed using the constant of equilibrium and coefficient of activity:

$$\lg K_{TiN} = \lg f_{Ti} [Ti] f_N^{Ti} [N] = -5674/T + 0.268,$$

where K_{TiN} is the constant of equilibrium of titanium nitride; f_{Ti} is the coefficient of titanium activity; f_N^{Ti} is the coefficient of nitrogen activity in the presence of titanium.

In work [1]

$$\lg f_{Ti} = -0.935 [Ti] + 0.643 [Ti]^2,$$

$$\lg [N] = -2.795 + 0.935 [Ti] - 0.643 [Ti]^2 - \lg [Ti] + 0.45 [Ti],$$

consequently,

$$[N] = 10^{[-2.795 + 0.935 [Ti] - 0.643 [Ti]^2 - \lg [Ti] + 0.45 [Ti]]}.$$

Figure 1 gives the relationships between the nitrogen content in metal and content of aluminium and titanium, and Figure 2 shows the effect of temperature on equilibrium of aluminium–nitrogen and titanium–nitrogen systems in iron at 101.325 kPa partial pressure of nitrogen. It is seen from these relationships that decrease in concentration of a free nitrogen in the molten metal corresponds to more than 0.1 % titanium or 0.9 % aluminium content in it. Its exceeding leads to the formation of nitrides in the molten metal. The large nitrides are formed which are capable to escape to the slag. The nitrogen solubility in a solid metal (austenite) in the presence of aluminium and titanium is decreased. During cooling with a decrease in the temperature the fine-dispersed nitrides are formed in the metal, for example, formation of aluminium nitride:

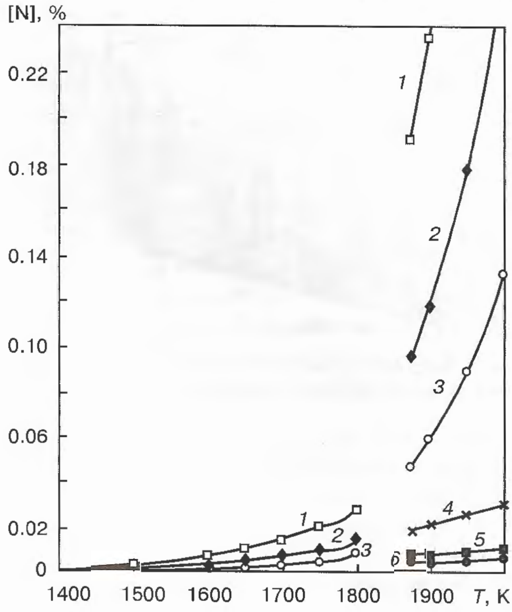

Figure 2. Diagram of aluminium–nitrogen and titanium–nitrogen equilibrium in iron, %: *1* — 0.25 Al; *2* — 0.50 Al; *3* — 1.00 Al; *4* — 0.10 Ti; *5* — 0.30 Ti; *6* — 0.50 Ti

$$AlN = Al_{(\%\ in\ austenite)} + N_{(\%\ in\ austenite)}.$$

The equilibrium solubility according to the above-mentioned reaction of nitrogen in austenite at 1.0 % aluminium and temperature 1500 °C is 0.021, and at 1100 °C it is only 0.001 %.

To study the effect of a complex alloying on structure of the weld metal, contained aluminium and titanium, the calculations of structure were made using a software, developed at the E.O. Paton Electric Welding Institute [4], which was aimed at the prediction of microstructure of a single-pass weld, formed during solidification of weld metal and its next cooling to the ambient temperature.

As a rule, the microstructure of low-alloyed steels at high rates of cooling, typical of welding, consists mainly of a mixture of an allotriomorphous (grain boundary) ferrite (AF), plates of Widmanstätten ferrite (WF), acicular ferrite (AcF) and a small amount of microphases.

The AF is the first phase which is formed during cooling below temperature A_r and implanted heterogeneously along the boundaries of colonies of austenite grains. Austenite transformation into AF occurs as a result of a diffusive redistribution of carbon and other elements dissolved in iron. At a further cooling the WF is implanted at the boun-

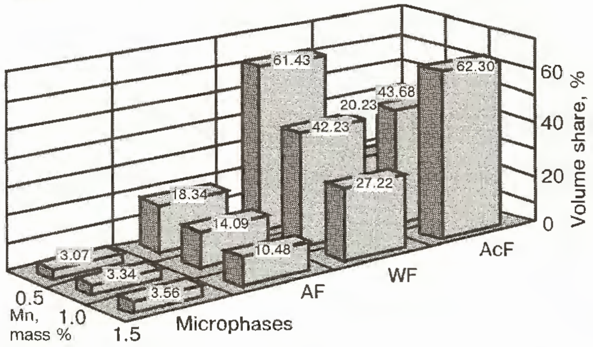

Figure 3. Relationship between the amount of structure constituents of weld metal and manganese content at 0.9 % Al

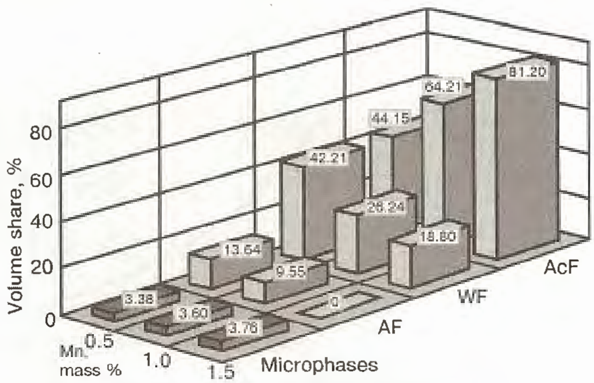

Figure 5. Relationship between the amount of structure constituents of weld metal and manganese content at 0.1 % Ti

dary of AF and austenite and preserved at lower and normal temperatures. Growth of WF is possible when there are conditions of accumulation of carbides in the direction of transformation. Morphology of AcF consists of non-parallel plates of ferrite inside the austenitic grains. Implantation of AcF plates on inclusions initiates the growth of non-parallel plates in many ordinary crystallographic directions caused by an initiated inclusion. On the contrary, the WF plates are formed of almost plane boundary of AF and austenite and, consequently, they are lined in parallel. The bainitic transformation is most probable when during the temperature decrease the region is attained, in which the rate of diffusion of atoms of iron and alloying elements is extremely low and the rate of carbon diffusion is still high. Due to a small sizes of needles and owing to their high-angular boundaries the AcF structure is most preferable for low-carbon non-alloyed and low-alloyed welds, as it provides both a sufficient toughness and strength of the weld metal.

Aluminium and titanium, which are not bound in nitrides, play the role of an austenizer. To intensify the austenite transformation it is necessary to introduce such ferritizers as manganese and nickel. At widening the γ-region and temperature decrease, such state is attained when the mobility of carbon in ferrite is decreased and disorientation of carbides with a formation of AcF of a disoriented bainite at presence of fine-dispersed inclusions is occurred. The presence of aluminium and titanium can cause the earlier precipitation of large oxides and nitrides in the weld pool, thus leaving a less amount of oxygen before the beginning of solidification for the formation of small oxides particles which can serve centres for nucleation of AcF. Role of nuclei can be played by dispersed nitrides.

In calculations the following content was taken, %: C — 0.10; Si — 0.30. The content of main alloying elements varied within the ranges, %: 0.5 – 1.5 Mn; 0.8 – 1.2 Al; 0.5 – 1.5 Ni; 0.10 – 0.20 Ti. The welding speed was taken equal to 3.6 mm/s cooling time (from 800 to 500 °C) was 3.92 s. Figures 3 – 6 give the calculations of the weld metal structure.

When alloying to 0.5 % Ni the increase in share of AcF occurs at the expense of decreasing the share of both AF and WF. Within the range from 0.5 to 1.0 % Ni it occurs mainly at the expense of decreasing the share of AF. This is, probably, associated with the fact that at small nickel concentrations it has a comparatively higher influence on the decrease of the growth rate of WF than in concentrations above 0.5 %. The more preferable structure of weld metal is attained at nickel and manganese content at the level of 0.7 – 1.0 and 1.2 %, respectively. The metallographic analysis confirmed the above-mentioned changes in shares of structure constituents of the weld metal.

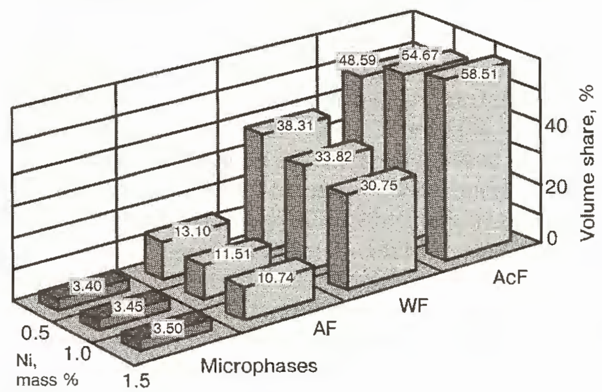

Figure 4. Relationship between the amount of structure constituents of weld metal and nickel content at 0.9 % Al and 1.0 % Mn

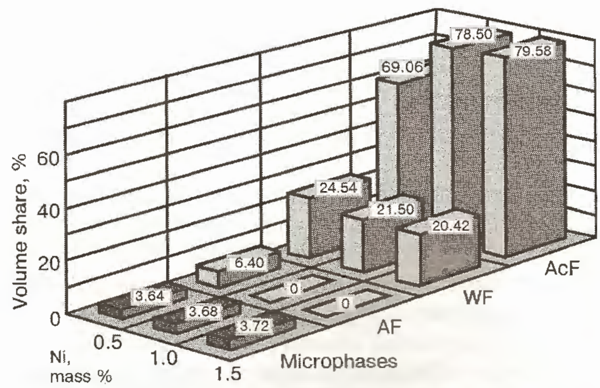

Figure 6. Relationship between the structure constituents of weld metal and nickel content at 0.1 % Ti and 1.0 % Mn

The data obtained indicate that at a basic alloying with nitride-forming elements of titanium and aluminium the introduction of nickel and manganese to the weld metal makes it possible to predict the volumetric share of the AcF. Thus, the results of model calculations can define the region of the weld metal with a favourable microstructure for the conditions of a self-shielding flux-cored wire welding.

CONCLUSIONS

1. Concentration of a free nitrogen in a solid metal at 101.325 kPa partial pressure is decreased with increase in content of titanium or aluminium in molten metal for more than 0.1 and 0.9 %, respectively. Increase in content of nitride-forming elements leads to the formation of large nitrides in the molten metal, which are capable to escape to the slag. Below the temperature of metal solidification the precipitation of dispersed nitrides in a solid metal is occurred.

2. To intensify the austenite transformation it is necessary to alloy metal with such ferritizers as manganese and nickel, because the aluminium and titanium are austenizers. When widening the region of $\gamma \rightarrow \alpha$ transformation, such state can be attained with a temperature decrease when the carbon mobility in ferrite is decreased and the disorientation of carbides with AcF formation and bainite disorientation occur at the presence of centres of solidification.

3. When alloying with aluminium and titanium the structure and properties of the weld metal can be regulated by a complex alloying with ferritizers which provide a larger share of a fine-dispersed structure constituent of the AcF type. The degree of alloying should be selected from the level of content of aluminium and titanium in the weld metal.

REFERENCES

1. Morozov, A.N. (1986) *Hydrogen and nitrogen in steel*. Moscow: Metallurgia.
2. Pokhodnya, I.K. (1972) *Gases in weld*. Moscow: Mashinostroyeniye.
3. Pokhodnya, I.K., Suptel, A.M., Shlepakov, V.N. (1972) *Welding with flux-cored wire*. Kyiv: Naukova Dumka.
4. Shlepakov, V.N., Kotelchuk, A.S. (1989) Estimation of structural composition of metal of low-alloyed welds made by flux-cored wire. In: *Information materials of CMEA*. Issue 1. Kyiv: Naukova Dumka.

FEATURES OF FERRITE BAND FORMATION IN VACUUM PRESSURE WELDING OF STEEL

S.I. KUCHUK-YATSENKO, G.K. KHARCHENKO, Yu.V. FALCHENKO,
T.G. TARANOVA and S.G. GRIGORENKO
The E.O. Paton Electric Welding Institute, NASU, Kyiv, Ukraine

Key words: *ferrite band, vacuum diffusion welding, vacuum percussion welding.*

The ferrite band (FB) several tens and hundreds of microns wide, is found in the microsections of steel welded joints produced by various pressure welding processes with heating in air (roll, gas pressure, furnace, air-contact) [1 – 6]. There is no common opinion on the mechanism of FB formation in published papers.

The publications mostly deal with two hypotheses which account for FB appearance in pressure welding with heating in air. According to one of them, FB forms as a result of the process of decarburization of near-contact metal volumes in heating prior to upsetting or at the deformation stage. In this case, FB width grows with the decrease of carbon content in steel. According to another hypothesis, FB forms in cooling of the welded joint as a result of the process of phase recrystallization, when the oxides elongated along the butt act as ferrite nucleation centers.

Analysis of publications shows that the mechanism and kinetics of FB formation have been so far insufficiently studied. The issues of FB formation in pressure welding under vacuum have not been considered in publications. The goal of this study was to generate new information on the features of FB formation in vacuum pressure welding of low-alloyed low-carbon steel.

Welded joints made by vacuum percussion (VPW) and vacuum diffusion (VDW) welding have been studied (Figure 1). The heating mode, welding temperature, cooling conditions and degree of plastic deformation were identical for both welding processes (t_1 is the time required for the billet heating to the welding temperature; t_2 is the soaking time at the welding temperature; t_3 is the welding time; t_4 is the cooling time; P is the upset pressure; W is the impact energy). During investigations the welding temperature was 1000 °C, since at the welding temperature below the temperature of $\alpha \rightleftarrows \gamma$ transformation, no FB is formed. The fundamental difference between these welding processes consists in the deformation time which in VDW is equal from several minutes to tens of minutes, and in VPW is of the order of 10^{-2} s [7, 8]. In VPW an anomalously high mobility of the atoms is found at the sample upsetting stage, at which the speed of atoms migration in the contact zone is by several orders of magnitude higher, than under the conditions of isothermal heating, and the recrystallization process proceeds at the cooling stage. In VDW, unlike VPW, the recrystallization and mass transfer processes occur at the upsetting stage.

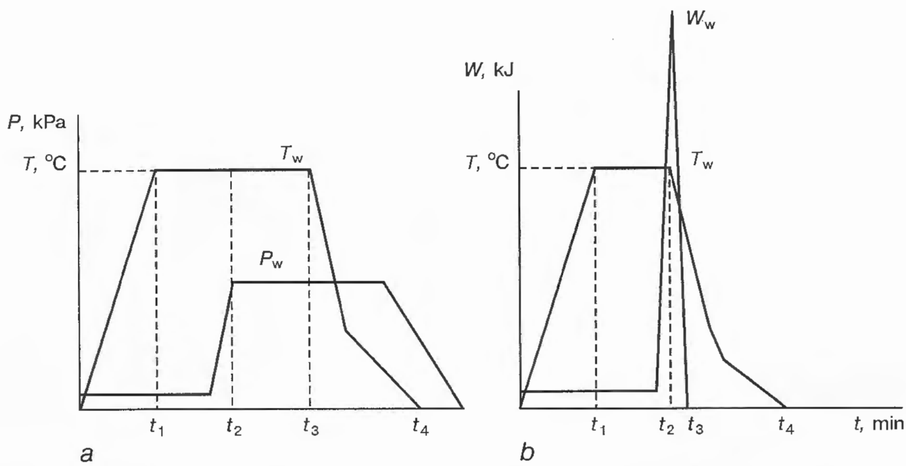

Figure 1. Cyclograms of the processes of diffusion (*a*) and percussion (*b*) welding under vacuum: $t_1 = t_2 = 5$ min; $t_3 = 5$ min (VDW); $t_3 = 10^{-2}$ (VPW)

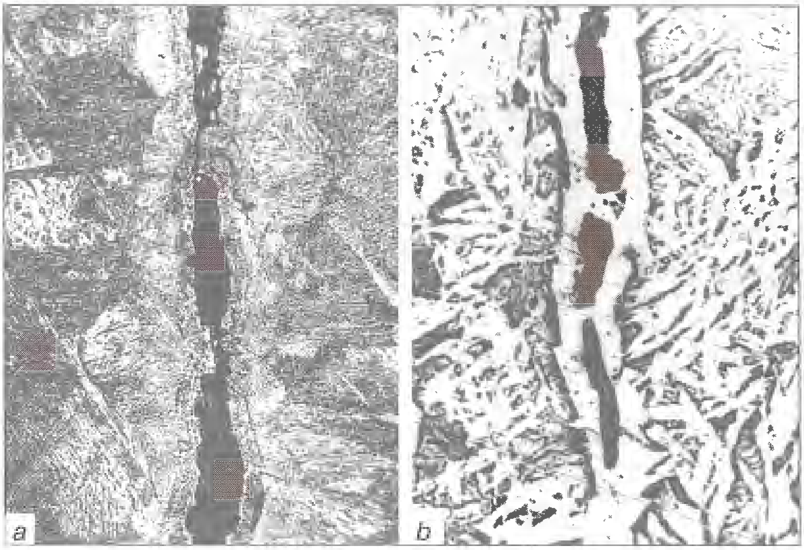

Figure 2. Microstructure of the contact zone formed at the heating stage before upsetting, at the oxide thickness of ~ 4 μm on one of the surfaces being welded: *a* — quenching in water; *b* — slow cooling under vacuum (×200) (reduced by 0.49)

It is known that during the steels heating up to 1000 °C under vacuum, the main process of reduction (metallizing) of the oxide on the metal surface, is carbon interaction with the oxygen of the oxide [9, 10]. Carbon has low volatility and can be removed from the metal only as part of CO or CO_2 gas molecules. Note that the depth of the decarburized zone on the steel surface, depends on the carbon content in steel, temperature and time of heating, as well as the oxide film thickness.

Investigation of the contact zone structure and the composition was conducted in the optical (Neophot-32) and scanning electron (JSM-840) microscopes. X-ray microprobe analysis («Camebax», SX50 model) was also used, in order to assess the content of oxygen, carbon, silicon and manganese. X-ray phase analysis of non-metallic inclusions in the contact zone was conducted in «Dron-3M» diffractometer. Oxide thickness of up to 4 nm was determined by Auger-electron spectroscopy. The microhardness of the joints was evaluated by microhardness tester of M-400 type of the LECO company (10 g load). Etching of microsections was performed in 20 % water solution of chromic acid.

Investigations were conducted on up to 15 mm thick and up to 60 mm long samples of low-alloyed low-carbon pipe steel of the following composition (weight fraction), %: C — 0.18; Mn — 1.5; Si — 0.42; V — 0.14; Ni — 0.04; Cu — 0.0044; S — 0.018; P — 0.014. Gas content in the metal was, %: [O] — 0.0075; [H] — 0.0005 and [N] — 0.0087.

Note that the pipe metal in as-delivered condition, has a banded ferrite-pearlite structure.

Sample preparation for welding consisted in the following. The abutted surfaces were subjected to finish turning so that they had the same dimensions and shape, were parallel to each other and normal to the sample axis. Prior to welding, the abutted surfaces of the samples were scraped and degreased. After such treatment the oxide film thickness on the surface was approximately 4 nm. Experiments were also conducted with the samples which had been soaked (~ 1 s) at 1000 °C in air prior to welding, which resulted in formation of ~ 4 μm thick oxide film.

Experiments were performed in U-394 M unit fitted with the systems of static (VDW) and dynamic (VPW) deformation. The sample welding mode was as follows:

welding temperature, °C	1000
impact energy (VPW), kJ	3
upset pressure (VDW), kPa	3
vacuum in the working chamber, Pa	$1.33 \cdot 10^{-3}$
upsetting, mm	5 – 10

The investigation procedure envisaged a separate study of the features of FB formation, both at the stage of heating prior to upsetting, and of high-temperature deformation. The structure of the contact zone was studied after the samples quenching in water and after their slow cooling under vacuum from the welding temperature to 100 °C at the rate of ~ 30 °C/min.

Heating prior to upsetting. The stages of heating prior to welding are the same for VPW and VDW (see Figure 1). The experimental procedure at this stage of investigations had the following features. The samples to be welded were placed between rigid supports which limited their elongation. In this case, the force of the samples clamping was up to 0.01 P_w, which ensured deformation and adhesion of individual microprotrusions on the abutted surfaces. The microstructure of the contact zone of the samples was studied, one of which had the initial thickness of the oxide of 4 nm, and the other 4 μm.

The performed investigations demonstrated the following. The contact zone has sections of lack-of-

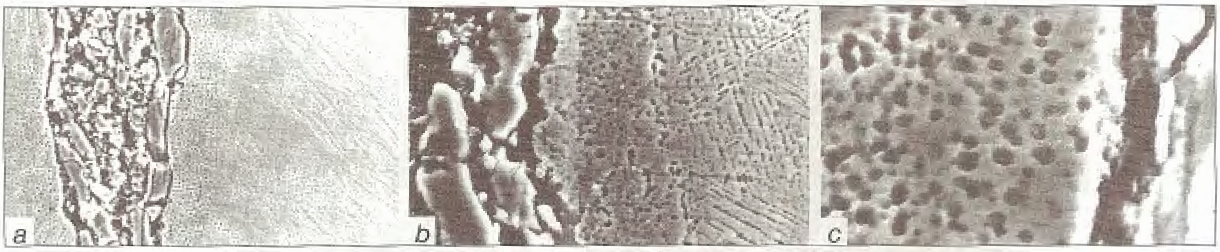

Figure 3. Microstructure of the contact zone of oxidised samples (oxide thickness of 4 μm), formed at the stage of heating prior to upsetting with quenching in water (*a* — ×1000; *b* — ×4000; *c* — ×8500) (reduced by 0.60)

penetration and of adhesion. No FB forms with the oxide thickness of 4 nm. It is only detected when the oxide on the surface of one of the samples is ~ 4 μm thick (Figure 2). After quenching the structure of the contact zone does not contain any FB (Figure 2, *a*). A similar structure was earlier observed in the pressure processes of steel welding in air [4]. During quenching, precipitation of structurally unbound ferrite is eliminated and all of austenite transforms into martensite. The interface in this case is detected only by different etchability of the surfaces being joined.

It is found that FB forms as a result of slow cooling of the contacting samples (Figure 2, *b*). Microstructural analysis allows the conclusion to be made that FB of equal thickness is formed on the surfaces of both samples in which the initial thickness of the oxide differs by several orders of magnitude. This is indicative of the fact that intensive oxidation of the sample which had a thinner oxide layer on the surface prior to welding, proceeds in the sealed microvolumes of the butt at the heating stage. Note that FB size becomes greater with the lowering of the cooling rate, while the contact zone structure after the samples quenching develops extensive zones of decarburization on the interface of the oxide and the metal. The results of investigation of the microstructure of the contact zone in an optical microscope lead to the conclusion that FB appearance around the perimeter of the sealed microvoids is related to the process of self-cleaning of the surfaces from the oxides [11], while the cooling rate determines its dimensions in keeping with the continuous cooling transformation diagrams of austenite decomposition [12].

As the optical microscope does not allow to reveal the contact zone structure in detail, analysis of the structure was performed using a scanning electron microscope (JSM-840). Figure 3 shows the microstructure of the zone of contact of quenched samples which as was earlier noted (Figure 2, *a*), had different initial thicknesses of the oxide on the surface. Study of the microstructure in the region of a closed sealed microvolume (lack-of-penetration) leads to the conclusion that sections differing from each other in their structure and composition are found in the contact zone. Remnants of the fragmented oxide film are present in the microvolume proper. Complex finely-dispersed oxides of alloying elements of not more than 5 μm size, are located between the matrix metal and the oxide film remaining in the butt. The width of the zone of these oxides precipitation is up to 15 μm. It is found that oxide inclusions of maximal dimensions are located near the oxide film, the inclusion dimensions becoming smaller in the direction from the oxide film into the metal bulk. It is known that the structure of such a type is formed under the oxide film as a result of internal oxidation of the metal [13, 14]. The internal oxidation zone (IOZ) is formed under the oxide film due to oxygen diffusion from the sample surface into the metal bulk, and of the alloying elements from the metal towards the contact zone. It is found that the metal matrix near IOZ is characterised by a lower content of the alloying elements. Note that no IOZ could be detected in the structure of the samples not subjected to heating after oxidation. Thus, IOZ is only formed at subsequent heating of the first oxidised samples.

The structure of the contact zone after slow cooling of the samples is indicative of the fact that the process of phase recrystallization of ferrite with FB formation on finely-dispersed oxide precipitations was completed at the cooling stage, in keeping with the continuous cooling transformation diagrams of austenite decomposition. FB width corresponds to the width of the area of finely-dispersed oxide precipitations.

Distribution of such elements as oxygen, carbon, manganese, silicon was studied in the contact of samples subjected to slow cooling and having FB in their microstructure. X-ray microanalysis revealed that oxygen concentration is almost two times higher at the oxide-metal interface than in the areas of adhesion of individual microprotrusions, while the content of manganese and silicon in the near-contact areas, is higher. The nature of carbon distribution could not be revealed in connection with its small content. It can be assumed that such a distribution of oxygen, manganese and silicon is related to the processes of self-cleaning of the surfaces during heating [11] and IOZ formation [13, 14].

Analysis of the above investigation results leads to the conclusion that if the sample surfaces are covered with a thin layer of oxide (~ 4 nm) before heating, oxide film reduction by the carbon of the

Figure 4. Microstructure of the zone of the joint produced by VDW with ~ 4 nm oxide thickness on the sample surface (×200) (reduced by 0.72)

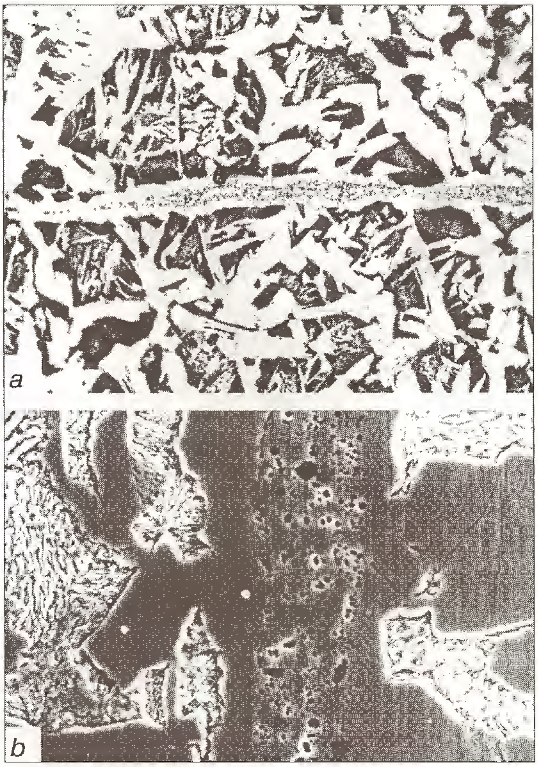

Figure 5. Microstructure of the zone of the joint of oxidised samples produced at the oxide thickness of ~ 4 μm: *a* — Neophot-32 camera (×200); *b* — JSM-840 (×1000) (reduced by 0.92)

metal proceeds at the heating stage, but the thus produced decarburized zone is so small, that it does not create any conditions for FB formation. If the sample surfaces are covered with a thick layer of oxide (~ 4 μm) before heating, FB forms in the contact after slow cooling of the samples, and that takes place on the surfaces separated by the remnants of the initial oxide film, as well as in those contact areas where metal joining in the solid phase took place. A short-time oxidation of the abutted surfaces (seconds) at the temperature of 1000 °C, does not lead to IOZ formation under the oxide film, but their high-temperature heating even of very short duration (5 min) leads to formation of IOZ which accumulates the oxides of the alloying elements. At the stage of heating of the oxidised surfaces, the process of oxide film reduction by the carbon of the metal, and, hence, decarburization of near-contact volumes take place, as well as oxygen interaction with manganese and silicon in IOZ, which results in formation in the butt of finely-dispersed non-metallic inclusions (MnO_2, SiO_2) of ~ 1 μm and complex oxides (Mn_2SiO_2) of a larger size. Phase recrystallization proceeds in cooling and FB is formed in the butt.

The issue of where the gaseous products of oxide reaction with carbon go from the sealed microvolumes oriented along the butt, is still not clear. It is known that during self-cleaning of the steel surface from the oxides, the reduced particles of iron oxide preserve their dimensions, transforming into highly-porous iron. Thus, it can be assumed that evolution of gas (CO, CO_2) not only into the vacuum, but also into the micropores with which the metal matrix is saturated, is quite probable [15]. This issue is not yet described in publications.

Upsetting stage. Let us consider the features of FB formation at the stage of upsetting and cooling, separately for VDW and VPW, as there exist essential differences between the studied welding processes as to the time of the high-temperature deformation running.

Vacuum diffusion welding. Investigation of the joint structure shows that in the case of welding samples with ~ 4 nm initial thickness of the oxide on the surface, FB does not form with the accepted modes of welding and cooling (Figure 4). Microstructure examination in the optical microscope revealed that no defects in the form of lacks-of-penetration or remnants of the oxide film are found in the joint zone. The process of metal recrystallization in the butt is completed at the upsetting stage and common grains are found in the place of the former interface.

The presence of FB in the structure of the joint produced by VDW, is only detected at slow cooling of the samples with ~ 4 μm initial thickness of the oxide on the surface. Non-metallic inclusions which by the data of X-ray microanalysis are complex oxides of alloying elements present in the steel composition, are found in FB central part (Figure 5).

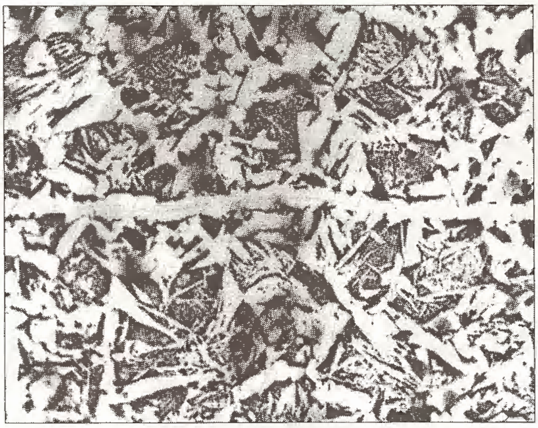

Figure 6. Mictrostructure of the zone of the joint produced by VPW with ~ 4 nm oxide thickness on the samples surface (×200) (reduced by 0.83)

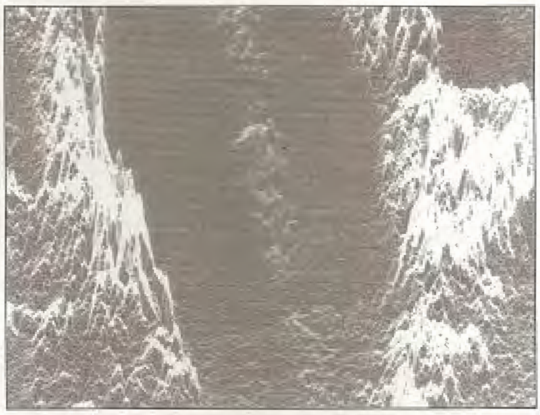

Figure 7. Microstructure in the back-scattered electron mode, of the zone of the joint produced in VPW with ~ 4 μm oxide thickness on the sample surface (×1700)

Vacuum percussion welding. We considered the features of FB formation in welding with 4 nm initial thickness of the oxide on the surface. Figure 6 shows a characteristic microstructure of the joint made by VPW. The investigation results indicate that FB width varies from several up to 30 μm, depending on the surface microgeometry, its cleanliness and joint cooling rate. It is found that lowering of the welded joint cooling rate leads to greater thickness of FB. It is shown that reduction of the height of microprotrusions on the samples surface decreases FB thickness down to its complete disappearance in the case of welding samples with polished surfaces.

FB microhardness is 1250 to 1270 MPa, while that of the matrix ferrite is 1330 – 1400 MPa. Thus, the ferrite of the band has a somewhat lower microhardness than that of the matrix. It is known that with the pressure processes of steel welding in air, the ferrite of the band has the microhardness somewhat higher than that of the matrix. The authors of [1 – 6] attribute that to oxygen dissolution in the weld zone. Therefore, the conclusion can be made that no saturation of FB with oxygen proceeds under VPW conditions.

X-ray microanalysis showed that the content of silicon and manganese in the butt and the matrix is the same, while the amount of oxygen became smaller than at the stage of preheating.

When FB structure is studied in the optical microscope, the so-called bright line is revealed in a number of cases, which, according to [4], presumably is the zone of maximal oxygen saturation. The nature of its formation was not considered in earlier publications. It is probable that optical microscopy detects the bright line due to that the oxides have a high reflectivity. Investigation performed in an electron microscope, showed that it is located in FB middle and consists of non-metallic inclusions which have a higher content of manganese, silicon, aluminium and calcium. With the total initial thickness of oxide film of ~ 8 nm on both abutted surfaces, the bright line thickness is from 1 to 2 μm, i.e. it is by several orders of magnitude greater. The following mechanism of FB formation in VPW can be assumed. During deformation, an accelerated mass transfer of the atoms of elements present in the steel composition and their interaction with oxides present on the abutted surfaces, proceed in the contact zone, this resulting in the formation of a decarburized zone with finely-dispersed non-metallic inclusions located along its center. FB forms on these inclusions in cooling of the welded joint.

In vacuum welding only the VDB process does not lead to FB formation in the structure of a joint of samples with ~ 4 nm thickness of the oxide. As noted above, VDW process fundamentally differs from VPW process in that in VDW recrystallization proceeds at the upsetting stage in the time interval which is by several orders of magnitude longer than the time of deformation in VPW. The known processes of pressure welding with metal heating in air, are also characterised by an immeasurably small, compared to VDW process, time of high-temperature deformation. Thus, VDW process can be compared with the process of welded joint normalising. In [1 – 6] it was found that normalising (900 to 1000 °C temperature, up to 30 min soaking time) of welded joints leads to FB elimination from the joint structure. Here, non-metallic inclusions oriented along the butt, are not redistributed, but disguised, to use the terminology of [2], by the growing crystals which eliminate the initial flatness of contact of the elements being joined, by formation of common grains between them. The influence of metal recrystallization in the contact zone on the joint structure is demonstrated by the results of the following experiments.

VPW of samples was conducted, which was followed, without relieving the load, by soaking the joint at the temperature of 1000 °C for 5 to 10 min (VDW mode). After cooling of such a joint, no FB was found in its structure. However, if annealing ($T > \alpha \rightleftarrows \gamma$, $v_c = 120$ °C/h) of the welded joint is to be conducted in keeping with recommendations of [2], favourable conditions will be in place for FB formation on non-metallic inclusions oriented along the butt.

The results of the performed investigations lead to the assumption that FB formation in solid-phase welding of steels with heating, is due to a set of processes proceeding at the stages of heating, upsetting and cooling. These processes can conditio-nally be defined as diffusion and recrystallization. The diffusion processes, namely self-cleaning of contacting surfaces from oxides, mass transfer in the contact and interaction of elements present in the steel composition, with oxygen, lead to decarburization of the near-contact volumes and formation of internal oxidation zone in them, in which non-metallic inclusions are located. Recrystallization processes are the intergrowth of the crystallites through the initial contact surface and phase recrystallization of the metal in its cooling after welding.

CONCLUSIONS

1. The ferrite band is formed as a result of several processes proceeding at the stages of heating, upsetting and cooling. A mechanism of FB formation as an integrated action of the diffusion and recrystallization processes is proposed.

2. The processes of oxide film reduction by the carbon of the metal and oxygen interaction with the alloying elements of steel, decarburization of the near-contact volumes and formation in the butt of finely-dispersed non-metallic inclusions of ~ 1 μm (MnO_2, SiO_2) and complex oxides (Mn_2SiO_4) of a larger size, proceed at the stage of the oxidised surfaces heating.

3. Short-term oxidation of the abutted surfaces (seconds) at the temperature of 1000 °C does not lead to formation of IOZ under the oxide film, but their high-temperature heating, even of a short duration (5 min), leads to formation of this zone in which the alloying element oxides are concentrated.

4. FB can be detected in the structure of VDW joint only at slow cooling of the samples with ~ 4 μm initial thickness of the oxide on the surface. Non-metallic inclusions are found in FB central part.

5. In VPW FB forms in the butt even at minimal thickness of the oxide. Here, its width is from se-veral up to 30 μm and varies depending on the surface microgeometry, its cleanliness and joint cooling rate. A bright line 1 to 2 μm thick, consisting of non-metallic inclusions, is located inside FB.

REFERENCES

1. Astrov, E.I. (1960) Mictrostructure and strength of the joints in pressure welding of multilayer steels. *Svarochnoye Proizvodstvo*, **2**, 21 – 24.
2. Polosukhin, N.A. (1952) *Structure and strength of gas pressure joints*. Moscow: Mashgiz.
3. Vladimirskii, T.A., Lozinskii, V.N. (1964) On the influence of deformation conditions in gas-pressure welding of carbon steels on the joint quality. *Svarochnoye Proizvodstvo*, **12**, 15 – 18.
4. Falkevich, A.S. (1952) Conditions of formation and properties of ferrite band in pressure welding processes. *Avtogen. Delo*, **8**, 8 – 12.
5. Matveev, Yu.M., Oshchenkov, Yu.P., Zubareva, A.A. *et al.* (1970) On the nature of the light-coloured band in the pipe weld produced by furnace welding. *Svarochnoye Proizvodstvo*, **8**, 9 – 10.
6. Iserson, K.G., Chernov, V.P., Mednikov, Yu.A. *et al.* (1974) On inhomogeneity of carbon and nickel distribution in the zone of the pipe weld produced by the furnace welding process and weld quality control. *Ibid.*, **4**, 10 – 11.
7. Shevchuk, T.V., Kharchenko, G.K., Karakozov, E.S. (1981) Formation of the joint in vacuum percussion welding. *Avtomaticheskaya Svarka*, **12**, 31 – 35.
8. Larikov, L.N., Falchenko, V.M., Mazanko, V.F. *et al.* (1974) Features of mass transfer in solid-phase welding of armco-iron under pulsed loading. *Ibid.*, **5**, 19 – 21.
9. Cherepnin, N.V. (1973) *Sorption phenomena in vacuum systems*. Moscow: Sov. Radio.
10. Ashkinazi, L.A. (1987) *Vacuum for science and technology*. Moscow: Nauka.
11. Kuchuk-Yatsenko, S.I., Kharchenko, G.K., Falchenko, Yu.V. *et al.* (1998) Self-cleaning of the abutted surfaces from oxides in solid-phase welding with heating. *Avtomaticheskaya Svarka*, **2**, 16 – 23.
12. Novikova, D.P. (1989) *High-temperature metallography of welded joints*. Kyiv: Naukova Dumka.
13. Malinochka, Ya.N., Shmelev, Yu.S., Olikhova, M.A. *et al.* (1981) Oxide formation in solid steel at oxygen diffusion into it. *Izv. AN SSSR, Metally*, **5**, 110 – 119.
14. Kofstad, P. (1969) *High-temperature oxidation of metals*. Moscow: Mir.
15. Cheremskoy, P.G., Slezov, V.V., Betekhtin, V.I. (1990) *Pores in solids*. Moscow: Energia.

OPTIMIZING OF COMPOSITION AND TECHNOLOGICAL PROPERTIES OF ELECTRODE WIRE Sv-08KhG2SNMT FOR SHIELDED-GAS WELDING OF HEAT-TREATED LOW-ALLOYED HIGH-STRENGTH STEEL

P.P. PROTSENKO and **N.T. PRIVALOV**
The E.O. Paton Electric Welding Institute, NASU, Kyiv, Ukraine

ABSTRACT

The influence of main alloying elements in the wire on the effective ionization potential of the arc atmosphere and the thermodynamic activity of elements in multicomponent iron-based melts is considered. Welding and technological properties of Sv-08KhG2SNMT electrode wire were studied in comparison with series-produced wires. It is shown that complex alloying of the wires with chromium, nickel, molybdenum and titanium within optimum limits in a wide range of test temperatures provides a high impact strength of the weld metal which is attributable to its favourable structure.

Key words: *low-alloyed steels, shielded-gas welding, welding wire, arc stability, metal spattering, formation of welds, properties of welded joints, investigations.*

Low-alloyed structural steels found a wide spreading in automobile industry and chemical machine-building, ship-building, pipe manufacture and industrial engineering. In many cases, in manufacture of isothermal vessels for storage and transportation of liquified gases and oil products in particular, it is rational to use the sparsely-alloyed heat-hardened steels of 09G2S and 09G2SYuCh type with an yield strength of $\sigma_y \geq 450$ MPa [1 – 5], which are produced by a domestic industry. Meanwhile, in arc welding of these steels the HAZ metal is weakened under the action of a thermal cycle and the mechanical properties of weld metal made with series-produced electrode wires of Sv-08G2S, Sv-08GSMT, Sv-08G2SMA and other grades, are deteriorated.

To eliminate or to decrease the HAZ metal weakening the welding of low-alloyed steels should be made at optimum thermal cycle that provides a fast heating of the parent metal, minimum time of its staying at elevated temperatures and a low rate of cooling the welded joint. The equal strength of weld and parent metal can be attained at the expense of an appropriate its alloying from an electrode wire. However, the systematized information about the effect of alloying elements, introduced into the electrode wire, on the characteristics of processes of arc welding of low-alloyed steels is limited and concerns mainly the influence of separate elements, but not of their combinations.

On the basis of generalized literature data and investigations carried out the present article describes the peculiarities of design of composition and technological properties of a complex-alloyed electrode wire Sv-08KhG2SNMT for a mechanized arc welding of heat-treated low-alloyed steels of an increased strength. It should be noted that this wire was developed at the Department No. 15 of the E.O. Paton Electric Welding Institute under the supervision of Prof. V.V. Podgaetsky.

The electrode wires developed for a shielded-gas welding should meet the following main technological requirements:

stable arc burning and minimum metal spattering within the wide range of parameters of welding in CO_2 and argon-based mixtures;

favourable formation of welds;

required mechanical properties of weld metal at temperatures from +50 to –70 °C;

absence of pores, crystalline and cold cracks in weld metal;

minimum evolution of welding aerosols;

low cost of wire and feasibility of its industrial manufacture.

To evaluate the stability of arc burning using different electrode wires, an electron analyzer of non-stationary processes and high-speed filming of the welding process, synchronized with an oscillographing the condition parameters were used [6]. A maximum length, whose exceeding leads to its breaking, served a criterion of arc burning stability [7]. Thermodynamic activity of alloying elements in multicomponent iron-based melts was studied by the methods of measurement of electromotive forces and isothermal calorimetric measurements

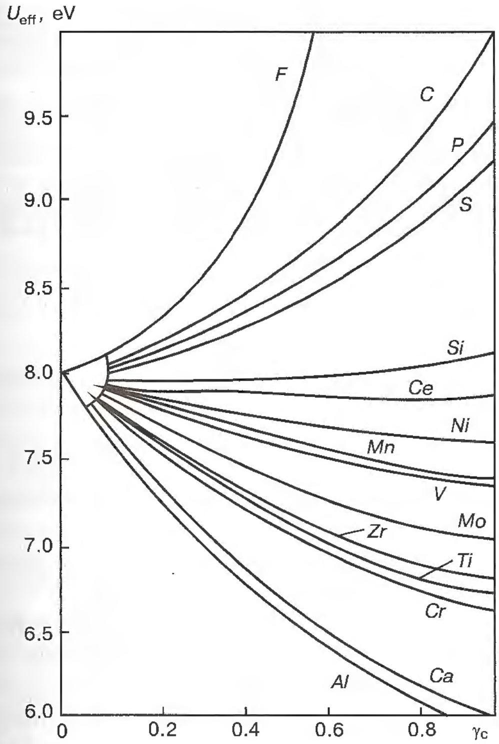

Figure 1. Effect of alloying elements on effective potential of ionization of two-component iron-based systems (T = 7000 K, P = 0.1 MPa)

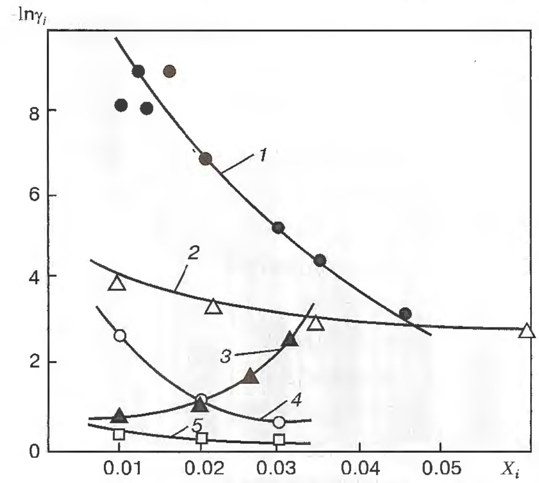

Figure 2. Relationship between the coefficient of activity (value $-\ln\gamma_i$) and concentration of alloying elements in iron-based melts: *1* — silicon; *2* — aluminium; *3* — molybdenum; *4* — manganese; *5* — chromium

described in [8]. The level of electrode metal spattering, coefficients of melting and deposition were determined by a gravimetric method. Structure and mechanical properties of weld metal were investigated using traditional methods. Sanitary-hygienic characteristics of electrode wires were measured by intensity of evolution of aerosols and their gross evolutions [9]. For this, a method of an inner filtering of aerosol on cloth FPP-15 and AFA-KhA-20 filters of air flow, aspirated from the welding zone shield was used.

As is known, an indirect characteristic of the arc burning stability is an effective potential of arc atmosphere on which the main characteristics of arc column and its near-electrode regions are depended. With use of a refined equation of Sakha [10] the concentration and temperature relations U_{eff} of two-component iron-based systems were calculated in computer (Figure 1). As is seen from Figure, the elements investigated can be divided into three groups by the degree of effect on U_{eff}:

elements, that reduce U_{eff} of binary systems (aluminium, calcium, chromium, titanium and zirconium);

elements, that do not influence greatly U_{eff} (silicon, zerium, nickel, manganese, vanadium and molybdenum);

elements, that increase U_{eff} (carbon, phosphorous, sulphur and fluorine).

It should be noted that a positive effect of aluminium and titanium on the stability of the process of CO_2 welding was discovered by V.I. Uljanov [11]. The effective influence of calcium as an active element was noted in [12], and that of chromium and zirconium — in [13, 14]. No single-valued relation between the effective potential of ionizing the arc atmosphere (Figure 1) and characteristics of transfer of electrode metal alloyed with appropriate elements [6] was observed. Probably, the latter affect not too much on physical processes in the arc, but mainly on the surface tension of the molten metal on which the sizes and frequency of electrode metal drop transfer are depended.

The experiments showed that the thermodynamic activity of each alloying element a_i is essentially changed when other alloying elements are introduced into the iron melt [8]. Thus, the presence of 99 % Fe + 1 % Si + 2 % Mn in the melt increases the activity of silicon by 2.2 times. In three-component system 97 % Fe + 1 % Si + 2 % Mn the addition of 1 % Ni increases a_{Si} by 14 times. Molybdenum increases a_{Si} by 215 times, and titanium and aluminium — by 16 and 19 times, respectively. The above-mentioned alloying elements increase also the manganese activity. The relations of coefficients of activity (γ_i) of silicon, aluminium, molybdenum, manganese, chromium in iron melts, generalized on the basis of [8], indicate (Figure 2) that silicon has the highest value of characteristic $-\ln\gamma_i$. It is followed by aluminium, molybdenum, manganese and chromium. With increase in content of components in complex-alloyed iron melts, only the molybdenum thermodynamic activity is increased.

As a result of investigations and comprehensive welding-technological tests, such a system of alloying the welding wires was selected as basic which envisages the limitation of an upper limit of content of carbon, manganese and silicon to 0.1, 1.7 and 0.3 – 0.6 %, respectively, additional intro-

Table 1. Welding-technological properties of low-alloyed wires of 2 mm diameter (CO_2 welding)

I_w, A	U_a, V	Wire grade	n_d, s^{-1}	τ_{av}, ms	l_a, mm	α_m, g/(A·h)	α_{dep}, g/(A·h)	ψ_s, %	Weld appearance
250	26	Sv-08G2S	16	65	4	–	–	6.5	Satisfactory
		Sv-08KhG2SNMT	15	70	5	–	–	6.0	»
350	32	Sv-08G2S	8	115	7	17.0	15.0	12.0	»
		Sv-08GSMT	6	125	9	–	–	13.0	Unsatisfactory
»		Sv-08KhG2SNMT	10	120	12	17.5	15.8	10.0	Satisfactory
450	36	Sv-08G2S	12	90	10	20.2	18.6	8.0	Good
		Sv-08GSMT	10	105	13	–	–	10.0	»
		Sv-08KhG2NMT	10	110	15	–	–	10.0	Satisfactory
		Sv-08KhG2SNMT	15	95	15	20.6	19.2	7.0	Good
600	38	Sv-08G2S	28	30	16	24.2	22.5	6.5	Satisfactory
		Sv-08KhG2SNMT	36	28	20	25.0	23.4	6.0	Good

duction of chromium into the wire in the amount of 0.5 – 0.8 %, and also alloying additions of nickel (0.6 – 0.8 %), molybdenum (0.4 – 0.6 %) and titanium (0.05 – 0.12 %). The relatively low content of carbon and silicon was taken to increase the resistance of the weld metal to the formation of crystalline cracks and to improve its impact strength. Chromium, as manganese, increases the strength of weld metal and decreases the harmful effect of sulphur. Nickel and molybdenum in the selected concentrations provide high ductility of the weld metal at room and low temperatures. Microadditions of titanium serve modifiers of the weld metal structure. The electrode wire designed for arc welding low-alloyed steels in shielding gases was designated as Sv-08KhG2SNMT grade. The electrode wire of Sv-08KhG2NMT grade which differs from the wire of Sv-08KhG2SNMT grade by a lower silicon content (to 0.3 %) is more preferable for submerged arc welding of the same steels. The feasibility of using wire Sv-08KhG2NMT for

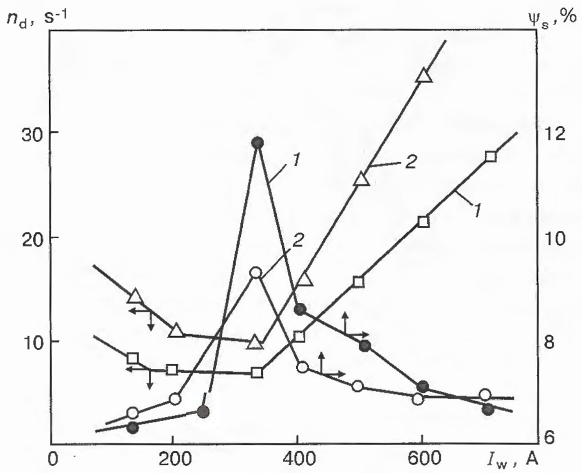

Figure 3. Relationship of frequency of drop transfer n_d (Δ, □) and coefficient of spattering ψ_s (○, ●) and welding current for 2 mm diameter wires Sv-08G2S (*1*) and Sv-08KhG2SNMT (*2*). Shielding gas – CO_2

submerged arc welding with fluxes AN-47 and AN-67 was grounded in [3, 4].

Comparative tests of electrode wires of different grades showed (Table 1, Figure 3) that the wire Sv-08KhG2SNMT, by its technological properties within the wide range of parameters of welding in CO_2 and Ar + 25 % CO_2, is not inferior to series-produced welding wires. The breaking length of arc l_a of complex-alloyed electrode wires is 1.3 – 1.5 times higher than that of the wire Sv-08G2S (Table 1). For all tested wires the metal losses for spattering are minimum and the formation of welds is more favourable in welding at relatively high (450 – 500 A) and low (250 A) currents that corresponds to the lowest time of drop staying at the electrode tip τ_{av} and highest frequency of their detachment n_d. The highest spattering (up to 13 %) and unsatisfactory formation of welds are observed in welding with wire Sv-08GSMT at medium current (about 350 A), when τ_{av} is maximum, and n_d is minimum. In all cases during CO_2 welding the diameter of drop d_d exceeds the electrode diameter. Coefficients of melting and deposition α_m and α_{dep} for wires Sv-08KhG2SNMT and Sv-08G2S are differed negligibly (Table 1).

The process of welding with wire Sv-08G2SNMT in CO_2 at low currents (to 250 A) at optimum arc voltage is proceeding with short-circuits of arc gap whose frequency is 12 – 16 drops per second (Figure 4, *a*). At currents above 250 and 350 A a mixed electrode metal transfer with short-circuits and free flight of drops take place (Figure 4, *b*). At transition to the forced conditions (I_w = 400 – 500 A) the electrode metal transfer occurs without short-circuits of the arc gap (Figure 4, *c*). At a further increase in current the arc is submerged into a pool and the spattering is decreased noticeably (Table 1, Figure 3). However, under these conditions when welding with wire Sv-08G2S the welds have a relatively high reinforcement and abrupt transitions to the parent me-

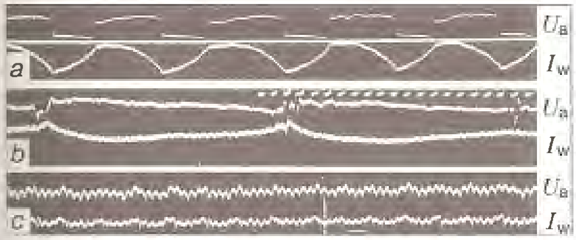

Figure 4. Typical oscillograms of electrode metal transfer in CO_2 welding with wire Sv-08KhG2SNMT of 2 mm diameter (designations $a - c$ — in a text)

tal. In this respect, the better formation of welds is provided by wire Sv-08KhG2SNMT that is explained by a good deoxidation of the molten metal and favourable effect of chromium and titanium on the arc burning stability.

During investigation of effect of composition of electrode wires on the properties and structure of weld metal the plates of the heat-hardened steels 09G2S and 09G2SYuCh of 10 mm thickness and V-shaped edge preparation were used. As a shielding medium, CO_2 and mixture Ar + 25 % CO_2 were used. Welding was performed in three layers using the following conditions: d_e = 2 mm; I_w = 400 – 420 A; U_a = 30 – 32 V; v_w = 30 m/h; $Q_{sh.g}$ = = 18 – 25 l/min.

The weld root was preliminary welded with 1.2 mm diameter wire of an appropriate composition at current 150 – 180 A and arc voltage U_a = = 18 – 20 V. The highest values of impact strength in the wide range of test temperatures were obtained in welding of heat-hardened steel 09G2SYuCh with wire Sv-08KhG2SNMT in an argon-based mixture (Figure 5). Somewhat lower

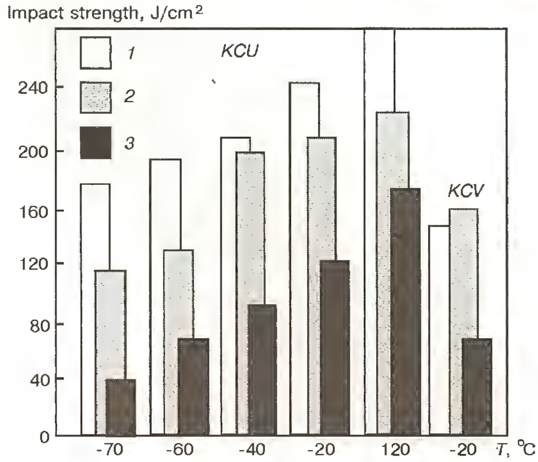

Figure 5. Impact strength of weld metal of welded joints of heat-hardened steel 09G2SYuCh made with wire Sv-08KhG2SNMT in mixture Ar + 25 % CO_2 (*1*), with the same wire in CO_2 (*2*) and with wire Sv-08G2S in CO_2 (*3*). Wire diameter is 2 mm; I_w = 400 – 420 A; U_a = 36 – 38 V; $Q_{sh.g}$ = = 20 l/min

values in impact strength were provided by the same wire in CO_2. In all cases the impact strength value is noticeably lower in CO_2 welding with wire Sv-08G2S. Similar effect of compositions of electrode wire and shielding medium is observed in welding of heat-hardened steel 09G2SYuCh.

Metallographic examinations showed (Figure 6) that in the process of a primary crystallization of welds made with wire Sv-08KhG2SNMT, the columnar crystallites formed are finer than those in weld metal made under similar conditions with wire Sv-08G2S. Attention is paid to the different direction of crystallites in the

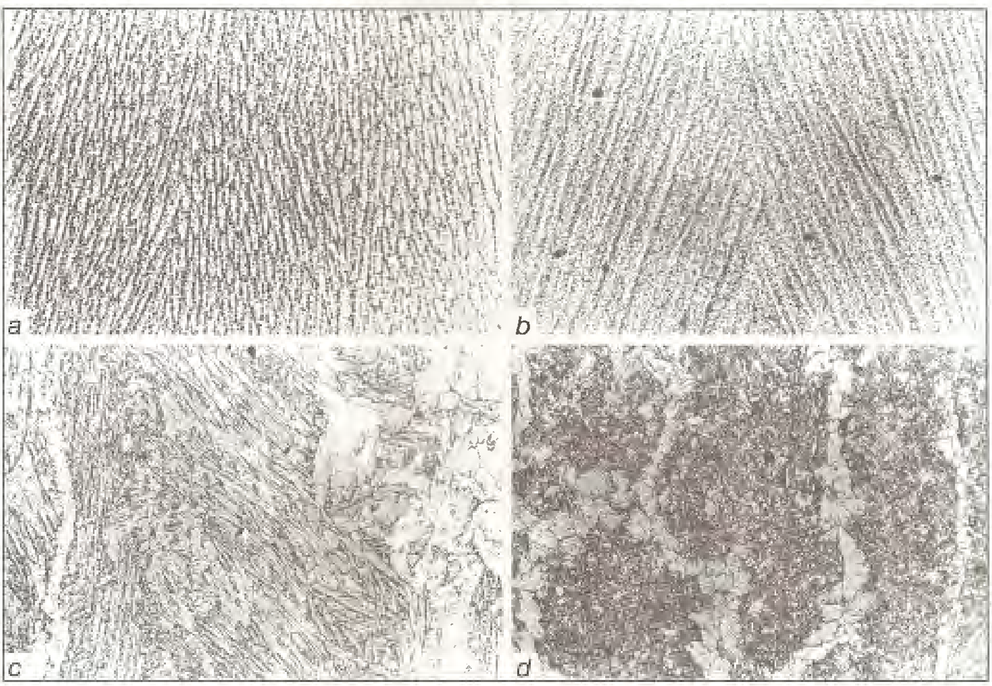

Figure 6. Primary (*a*, *b*) and secondary (*c*, *d*) microstructure of weld metal made on steel 09G2SYuCh with wire Sv-08KhG2SNMT (*a*, *c*) and Sv-08G2S (*b*, *d*) of 2 mm diameter. Shielding gas — CO_2 (*a*, *b* — ×50), (*c*, *d* — ×500) (reduced by 0.40)

Table 2. Comparative sanitary-hygienic characteristic of arc welding processes using different welding consumables

Electrode wire and its diameter, mm	Shielding gas	Flux	Welding conditions I_w, A	Welding conditions U_a, V	Intensity of HCWA formation, g/min	Specific evolution of HCWA, g/kg	Content of components in HCWA, % Mn	Si	Cr	F- dissolved	F+ undissolved
Sv-08G2S 2.0	CO_2	–	400	32	1.100	12.00	11.5	5.4	–	–	–
Sv-08KhG2SNMT 2.0	CO_2	–	400	32	0.800	9.00	9.5	5.3	0.03	–	–
Sv-08KhG2SNMT 2.0	Ar + + 25 % CO_2	–	400	32	0.500	6.00	6.2	4.0	0.02	–	–
Sv-08G2S 4.0	–	AN-67	720	38	0.047	0.26	16.4	9.8	–	4.8	3.2
Sv-08KhG2NMT 4.0	–	AN-67	720	38	0.042	0.20	15.2	9.0	Traces	5.4	3.3
Sv-08KhG2NMT 4.0	–	AN-47	720	38	0.035	0.22	16.8	8.9	»	4.2	3.8
Sv-08GM 4.0	–	AN-60	720	38	0.052	0.28	20.5	11.1	–	3.4	3.2
Sv-08A 3.0	–	AN-348	480	34	0.032	0.27	11.2	–	–	13.5	7.3

compared situations. The microstructure of weld metal of heat-hardened steel 09G2SYuCh is characterized by a presence of ferrite of a different morphology (acicular and flaky) and also of a small amount of martensite and bainite. In welding with wire Sv-08G2SNMT the share of the acicular ferrite is larger and the grain sizes are smaller than in weld metal made with wire Sv-08G2S. The great difference is observed also in a shape of non-metallic inclusions in weld metal made with different wires: for wire Sv-08KhG2SNMT the sizes of oxides are by one-two orders smaller than those for wire Sv-08G2S. On the basis of investigations, a chemical composition of electrode wire Sv-08KhG2SNMT was corrected for making the limiting content of alloying elements more precise.

Results of comparative tests of sanitary-hygienic characteristics of the mentioned electrode wires indicated that the intensity of formation and specific precipitations of hard constituents of welding aerosol (HCWA) in CO_2 welding with wire Sv-08KhG2SNMT is by 25 – 30 % lower than that in welding with wire Sv-08G2S (Table 2). This is explained by a lower content of manganese and silicon in it. The better sanitary-hygienic characteristics are observed in welding in Ar + 25 % CO_2 mixture. In all versions the intensity of formation and specific precipitations of HCWA in shielded-gas welding is greatly higher than in submerged arc welding with different combinations of wires and fluxes. However, the concentration of manganese and silicon in HCWA in submerged arc welding is higher than that in CO_2 welding and in Ar + + 25 % CO_2 mixture. In addition, in submerged arc welding the HCWA contains dissoluble and undissoluble fluorine. Remarkable precipitation of chromium in welding aerosols was not observed when welding in shielding gases and under the flux.

Under the experimental-industrial conditions the elements of the updated technology of manufacture of welding wires Sv-08KhG2SNMT and Sv-08KhG2NMT were tested at the stages of steel melting, hot rolling, heat treatment and drawing to the preset diameter. To reduce the losses of alloying elements and to improve the quality of steel an accelerated single-stage method of steel melting with a ladle treatment of molten metal and an accelerated technology of cooling the rolled wire to prevent excessive oxidation of its surface were suggested. Parameters of conditions of intermediate heat treatment of billet and routes of wire drawing to diameters 1.2 – 4.0 mm were optimized. Wires Sv-08KhG2SNMT and Sv-08KhG2NMT have passed the industrial tests at some enterprises of a chemical machine-building for welding isothermal vessels of heat-treated low-alloyed high-strength steels.

CONCLUSIONS

1. The composition of low-alloyed electrode wire Sv-08KhG2SNMT is peculiar by a limitation of an upper limit of content of carbon, manganese and silicon to 0.1, 1.7 and 0.3 – 0.6 %, respectively, by additional introduction of chromium to the wire in the amount to 0.5 – 0.8 %, and also of alloying additions of nickel, molybdenum and titanium.

2. It was established that additions of alloying elements (manganese, silicon, molybdenum, nickel) do not influence greatly the effective potential of ionization of the arc plasma. Chromium and titanium reduce U_{eff} and, thus, can increase the arc burning stability. Molybdenum in multi-

component iron-based melts have the greatest influence on the thermodynamic activity of alloying elements (silicon in particular). This shows a feasibility of more sparse alloying of steel, used for electrode wires, with silicon, chromium and other elements in the presence of molybdenum. The presence of a small amount of chromium (0.5 – 0.8 %) in steel increases the thermodynamic activity of molybdenum that makes it possible to consume this deficit and expensive component in smaller amounts (less than 0.6 %).

3. Within the wide range of welding parameters in CO_2 and mixture Ar + 25 % CO_2 the wire Sv-08KhG2SNMT, by all characteristics of technological properties (size of drops, their uniform transfer, level of spattering, coefficients of melting and deposition, weld formation and aerosol evolution), is superior to the series-produced welding wires Sv-08G2S and Sv-08GSMT by the similar characteristics.

4. The impact strength of weld metal (KCU^{-70}), made on heat-hardened steels 09G2SYuCh and 09G2S, reaches 170 J/cm^2 in welding in Ar + 25 % CO_2 mixture, and 110 J/cm^2 – in CO_2. In welding with wire Sv-08G2S in CO_2 this value does not exceed 30 J/cm^2.

5. Electrode wire Sv-08KhG2SNMT is recommended for shielded-gas welding of heat-treated low-alloyed high-strength steels. Wire Sv-08KhG2NMT is preferable for welding these steels in combination with fluxes AN-47 and AN-67.

REFERENCES

1. Asnis, A.E., Ivashchenko, G.A, Demchenko, Yu.V. (1983) Heat-hardened steel 09G2S with 450 MPa yield strength for welded structures. *Avtomaticheskaya Svarka*, **12**, 55 – 56.
2. Egorova, S.V., Sterenbogen, Yu.A., Yurchishin, A.V. *et al.* (1987) Weldability of low-alloyed steels hardened by normalizing from an intercritical interval of temperatures. *Ibid.*, **2**, 20 – 23, 31.
3. Privalov, N.T., Protsenko, P.P., Kozlovets, O.N. *et al.* (1999) Peculiarities of technology of welding of isothermal tanks of steel 09G2S using different combinations of welding consumables. *Ibid.*, **5**, 37 – 41.
4. Privalov, N.T., Protsenko, P.P., Kozlovets, O.N. *et al.* (1999) Application of steel 09G2SYuCh for manufacture of welded isothermal tanks. *Ibid.*, **6**, 33 – 37.
5. (1977) *Application of heat-hardened low-alloyed steels for objects of oil and gas industries*. Ed. by N.N. Koshelev. Moscow: Nedra.
6. Protsenko, P.P., Privalov, N.T. (1999) Effect of alloying elements on electrode metal transfer in shielded-gas welding. *Avtomaticheskaya Svarka*, **12**, 29 – 33.
7. Khrenov, K.K. (1949) *Electric welding arc*. Kyiv: Mashgiz.
8. Podgaetsky, V.V., Bondarenko, T.P., Privalov, N.T. *et al.* (1990) Activity of main alloying elements in low-alloyed steels for welding wires. *Avtomaticheskaya Svarka*, **6**, 15 – 18.
9. Golovatyuk, A.P., Levchenko, O.G. (1985) Values of gross evolutions of welding aerosols and their application in practice. *Svarochnoye Proizvodstvo*, **10**, 40 – 41.
10. Voropaj, N.M., Krivtsun, I.V. (1978) Effective potential of ionization of multicomponent systems with activating additions. *Avtomaticheskaya Svarka*, **2**, 66 – 67.
11. Uljanov, V.I. (1974) Effect of some alloying elements on technological characteristics of wires for CO_2 welding. In: *Thesis for Cand. of Techn. Sci. degree*. Kyiv: PWI.
12. Paton, B.E., Voropaj, N.M. (1979) Welding with activated consumable electrode in a shielding gas. *Avtomaticheskaya Svarka*, **1**, 1 – 7, 13.
13. Martynenko, S.A., Svetsinsky, V.G., Uljanov, V.I. *et al.* (1976) Wire with anticorrosion coating for welding in shielding gases. *Ibid.*, **9**, 53 – 54.
14. Asnis, A.E., Gutman, L.M., Pokladii, V.R. *et al.* (1982) *Welding in mixture of reactive gases*. Kyiv: Naukova Dumka.

IN A UNION WITH METALLURGISTS AND WELDERS — TO ENERGY-SAVING TECHNOLOGIES

B.E. PATON[1], **V.I. LAKOMSKY**[1], **B.F. PETROV**[2] and **A.S. KOROTYA**[2]
[1]The E.O. Paton Electric Welding Institute, NASU, Kyiv, Ukraine
[2]Open Joint Stock Company «Ukrainian Graphite», Zaporizhya, Ukraine

ABSTRACT

Experience accumulated by scientists of the E.O. Paton Electric Welding Institute and specialists of the Open Joint Stock Company «Ukrainian Graphite» in the area of energy saving in production of graphitized electrodes is described. A new design of the short power circuit of graphitizing furnaces, welded carbon material — aluminium contacts and technology for field welding of the short circuit are proposed.

Key words: *energy saving, graphitizing furnaces, short circuits, welded electric contacts, assembly welding.*

«Ukrainian Graphite» (Zaporizhya) is the only company in Ukraine which manufactures carbon products for needs of ferrous and non-ferrous metallurgy and which is a successor to the well-known Dneprovsk Electrode Factory (DEF). Founded under industrialization conditions early in the 1930s as an integral part of a high-capacity metallurgical complex, located on a base of the Dneprovsk Hydroelectric Station in the South of Ukraine, the Factory became one of the pioneers in the electrode sector of the non-ferrous metallurgical industry of the former Soviet Union. Initially, the Factory was part of the Dneprovsk Aluminium Works. Then, owing to successful development and expansion, in 1940 it was separated into an independent enterprise, which within the shortest terms became the USSR — largest manufacturer of the carbon-based electrode products.

At the beginning of the Great Patriotic War the process equipment of the Factory was evacuated to the Urals and its buildings were blown up. After liberation of Zaporizhya in October 1943, the restoration and reconstruction works were started at the Factory to resume its operation. In May 1945 the partially restored Electrode Factory provided metallurgists with the first products which were so needed at that time. In the 1950s the rapidly developing ferrous metal industry needed new carbon-based lining materials. During those years, for the first time in the USSR the DEF specialists started up production of lining blocks for blast furnaces. Since that time all blast furnaces in the USSR and many such furnaces abroad were lined using the DEF blocks.

Electrometallurgy of steel wanted a new generation of graphitized electrodes. For that reason, within the shortest possible terms the DEF started up production of large-size electrodes for high-capacity electric arc furnaces. As a result of expansion of the production base and application of new technologies during a period from 1960 till 1980, the Factory doubled its output and thus became the most profitable enterprise in its sector. The reconstruction and technical re-equipment costs paid back many times.

In the 1970–1980s the Factory was building new advanced facilities, along with the reconstruction of old workshops. An example is a unique complex which was put into operation with a purpose of production of carbon–carbon compositions and products on their base. Today this facility is an independent State-owned Factory «Uglecomposite». Late in the 1970s a blanking shop was built and put into operation for the manufacture of a unique material, i.e. high-strength fine-grained graphite, to meet needs of the manufacturing industries, in particular for electric-pulse treatment of metals. In the same period the Factory started manufacturing catalyst extensions «Graton» for electrolytic cells, which served to decompose amalgam used with a mercury method for production of alkali in chemical industry.

However critically we can assess today the success of the Factory in the 1970–1980s, the workers not without the pride remember that the DEF graphitized electrodes for steel-making furnaces were the first to be awarded the State Quality Medal.

By the beginning of the 1990s the Factory team faced two extremely important tasks:

to complete construction and put into operation a carbon blanking shop to implement almost all achievements up to date in terms of the hardware, which would ensure a substantial increase in technical level of the products intended for lining of aluminium electrolytic cells;

to reconstruct the shop for graphitizing the electrode billets by building a new facility equipped

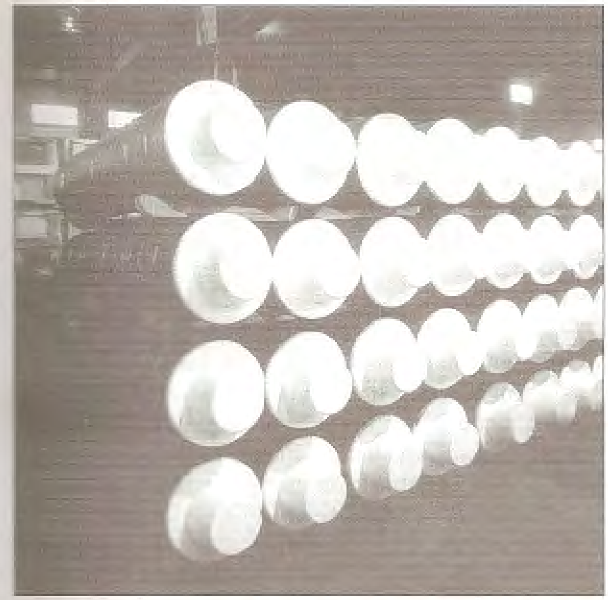

Figure 1. Graphitized electrodes prepared for shipment to Customers

Figure 2. Cathode units of aluminium electrolytic cells

with a new generation of electric resistance furnaces.

However, at that time the Factory turned out to have no funds for capital construction, no raw materials, as well as no information and research base. Main suppliers of raw materials and customers of finished products found themselves to be on the other side of frontier of our country.

After corporative changes in 1994, the DEF was transformed into the Open Joint Stock Company «Ukrainian Graphite», the founder of which was the state. Under extremely difficult conditions of non-payments and dramatic decrease in the number of solvent customers, the team of the factory managed to do the impossible: in 1996 the Company commissioned at its own expense a new unique shop for making coal billets with a fully automated part of the production cycle for making semi-finished products, based on the in-house electro-calcinated anthracite with controlled technical characteristics, which provided the consistent quality of cathode units for aluminium electrolytic cells and fundamentally improved their performance.

Imparting a paramount importance to quality of its products to be a success in the market, in 1997 the Company re-arranged its management structure by establishing the quality assurance service, whose main task was to introduce the system of international standards of the ISO 9000 series to ensure the consistent quality of the products. At present the products of the Company include:

graphitized electrodes with a diameter ranging from 75 to 710 mm and length of up to 2400 mm, with biconical nipple connections (Figure 1);

amorphous cathode units (30 % graphite + + 70 % electro-calcinated anthracite) with a cross section of 400×550 mm and length of up to 3700 mm (Figure 2);

bulk materials (anode, electrode, carbon, hearth);

carbon-graphite and graphitized lining blocks with cross sections of 550×550 and 400×400 mm for blast and other electric thermal furnaces (Figure 3);

various customized shaped items of carbon materials.

It should be noted that the manufacture of carbon products is a very power-consuming business. The power costs incurred by the Company in 1999 constituted 29.76 % of its total expenses, which in terms of money made 37.4 mln hryvnias. The power consumption is especially high in the manufacture of products of graphitized materials. The graphitizing process alone, which is performed at the factory in 100 kA Acheson-type furnaces, constitutes 55 – 58 % of the entire costs, excluding the costs of raw materials.

The quality of the products being the main priority, the Company is constantly looking for ways of reducing power consumption. This is especially topical today, as power saving in Ukraine, in the opinion of President L.D. Kuchma, is now «the issue of the national security». Analysis of power consumption in graphitizing carbon products shows that 9.4 to 19.6 % of power are lost to overcome electrical resistance of clamping contacts at the front and rear ends of the graphitizing furnaces in transition of the electric power from metal busbars of the short circuit to the graphitized current conductors which feed the current to the furnace [1]. Up to 30 % of the total capacity of the graphitizing furnaces are reactive losses in their short circuits.

In this connection, engineering and technical staff of the Company in collaboration with scien-

Figure 3. Graphitized lining blocks

tists of the E.O. Paton Electric Welding Institute have undertaken the task of finding the way for decreasing power consumption of the process of production of graphitized electrodes — one of the main products of the Company.

As the first step, it was necessary to solve the problem of replacing the low-amperage clamping contacts «metal–carbon material» by the welded ones, since the latter are characterized by a much lower contact resistance, which does not depend upon the service life of the contacts.

The clamping contacts of two solid bodies never touch each other over the entire visible surface of the connection. In the best case the actual contact may take place on the area which is 20 – 30 % of the visible surface for a metallic contact pair and only 8 – 10 % for a carbon material — metal contact, as the clamping force in the contact pair is limited by brittleness of the carbon material. The main drawback of the clamping contacts of the graphitizing furnaces is that the contacting surfaces are exposed to air and cooling water, which cause their rapid oxidation during an increased-temperature operation of the contact. In the graphitizing furnaces the temperature of the electric contacts, despite their cooling, amounts to 500 – 600 K. Because metal oxides are characterized as a rule by a higher electrical resistance than their metals, resistance of the contacts catastrophically grows with time. Thus, resistance of the clamping contacts «copper–graphitized carbon material» of the Company graphitizing furnaces during their operation increases from 100 – 150 to 15000 μOhm.

Welded contact connections can serve as an alternative to clamping contact [2, 3]. Welding of graphitized materials to metals is more than 25 years old. The commercially applied methods are intended for diffusion bonding and soldering, with the primary application in electronics. In this case joining is performed in vacuum or gas-filled chambers. Of course, these methods are unsuitable for making welded electric contacts in large-sized pieces, such as current conductors to graphitizing furnaces 400 × 400 × 1600 mm in size.

On this basis, the Centre for Plasma Technologies of the PWI, situated in the same city as the Company, developed a new plasma-arc method for welding carbon materials to metals in open air, using no gas or slag shielding. This method is unique and has no analogues in the world.

As in welding of a contacting pair the joining process occurs at a level of atomic interaction, the actual contacting surface in such a contact is equal to the rated (visible) one, which leads to a decrease in resistance of transition of the electric current and, therefore, to a reduction of the electric power losses. For the same reasons the contact connections with the welded contacts can be larger in size than those intended for the same currents but with clamping contacts. However, the main advantage of a welded contact (which puts it beyond any competition with the clamping contacts) is that the interface of its contacting pair is insulated from air. That is why, it can work at increased temperatures without a risk of oxidation of its mating surfaces and, hence, without an increase in electrical resistance of the contact.

To make such a welded contact it was necessary to overcome a number of difficulties associated with mutual weldability of different materials. The main problem was in a large difference in melting points of the materials joined. Carbon materials are known to melt at $T \approx 4000$ K, while such metals as iron, copper and aluminium, which are used to make bus ways, melt at 1812, 1356 and 932 K, respectively. A still large problem is in difference in thermal expansion coefficients (TEC) of the materials joined. Carbon materials used in electric metallurgical plants, despite their large diversity, have TEC within a range of $(3.0 - 4.5)\cdot10^{-6}$ K^{-1}. At the same time, TEC of the materials which are welded to carbon materials is much higher: carbon steel has TEC of $(11 - 13)\cdot10^{-6}$, copper — $17.6\cdot10^{-6}$ and aluminium — $22.8\cdot10^{-6}$ K^{-1} (all values correspond to room temperature).

These problems were solved using the specially developed technology for welding of individual metal plugs with a diameter and height of 30 mm into the bulk of a carbon material. Plasma-arc torches, i.e. arctrons, developed by the PWI were used as the welding heat sources [4]. The arctrons provide a rapid heating of the welding zone in a massive graphitized electrode which has a sufficiently high thermal conductivity, and, at the same time, do not allow oveheating of the locally liquid plug metal, which is a special electric-contact alloy, thus eliminating selective evaporation of individual

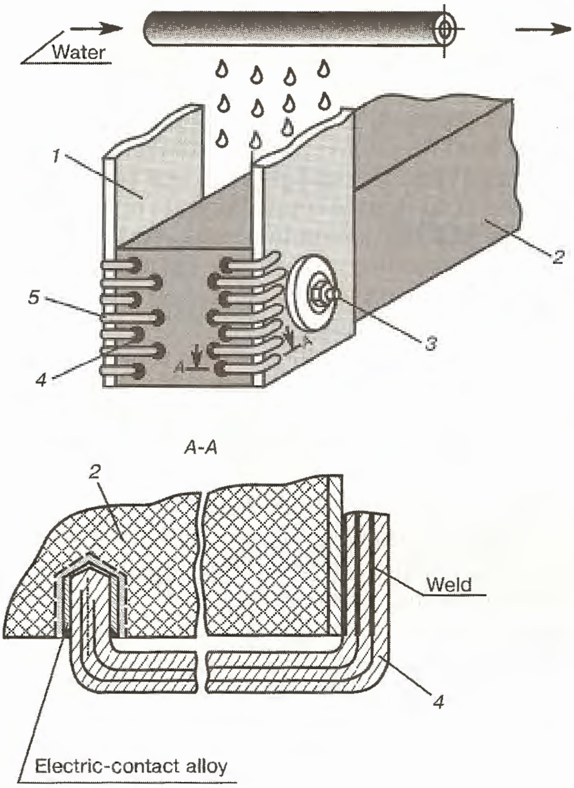

Figure 4. Diagram of a welded contact connection of one of the current-conductors for 11 kA to the graphitizing furnace with aluminium busbars. ECPs are welded into the end of the current conductor. Cooling is open, spray-type: *1* — aluminium busbars; *2* — current conductor of graphitized me-tal; *3* — pin; *4* — aluminium compensators; *5* — ECP

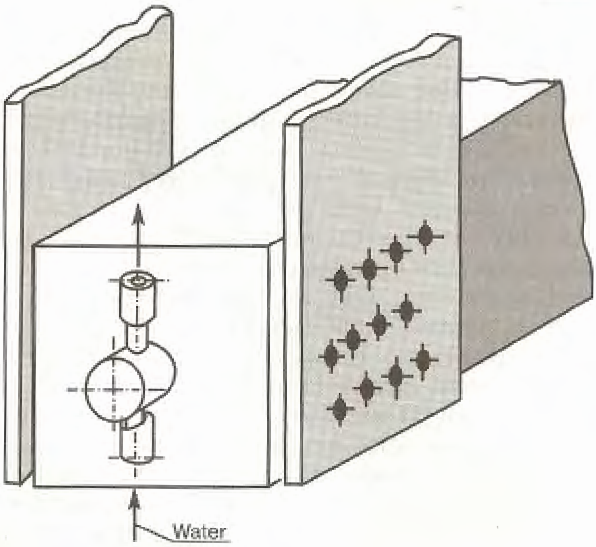

Figure 5. Same as in Figure 4, but ECPs are located on lateral ends of the current conductor. Cooling is of the closed type

components of this electric-contact alloy [2]. The electric-contact plug (ECP) welded into the carbon material is very strongly connected to the latter. It was experimentally proved that the force required to pull the plug out from the carbon material was 5000 –7000 N, fracture of the joint occurring not in the metal alloy but in the base carbon material.

ECPs are the basic design elements of all welded electric-contact connections. Depending upon the chemical composition of the electric-contact alloy and operation conditions of the plugs, each plug is designed for a current of 400 – 800 A. The plug is joined to the metal busbar using small-section metal rods (compensators), which are frozen-in into the plug prior to metal solidification, while the other ends of the rods are welded to the busbar by a conventional method (Figure 4). As can be seen from this Figure, 14 plugs are welded into the end of current conductor *2*, 400 × 400 mm in size, and metal busbars *1* bear against the current conductor using pin *3*. Compensators *4* in the form of flexible rods compensate for variations in sizes of the carbon material electrode and metal busbar during heating and cooling of the contact connection. This principle of making electric connections can be used to design contact connections of almost any dimensions.

Further on, in addition to the end clamping welded ECPs, the tests were also conducted to try out lateral plugs welded into the carbon material and, at the same time, to the aluminium busbar (Figure 5). Despite the use of shorter compensators, these current conductors provide good smoothing out of different thermal variations in the carbon material and aluminium at a compensator length of only 15 mm.

It should be noted here that the use of welded joints between carbon materials and metals makes it possible to overcome a stereotype of non-applicability of aluminium in contacts with carbon materials, which was formed in the course of utilization of clamping metal–carbon contacts at increased temperatures. The welded contacts, unlike the clamping ones, operate reliably at temperatures of up to 600 K. Therefore, using welding, the entire short circuit of the graphitizing furnaces can be made from aluminium. This makes it possible to fully exclude copper from the short circuit, as this is an expensive, heavy and not readily available material for Ukraine.

In reconstruction of the graphitizing furnaces at the «Ukrainian Graphite», the clamping contacts «copper–graphite» were replaced by the welded contacts «aluminium–graphite», and copper busbars were replaced by aluminium busbars. This allows saving of up to 150 kW·h of electric power per each ton of graphitized products (not saying about replacement of copper by aluminium), as well as saving of labour for cleaning and tightening of contacts.

The ECPs made on the carbon material, which has a certain porosity, are characterized by the fact that the impregnation zone is located as a rule near the cast zone of the welded-in plug in the carbon material. During the welding process the plug metal, having a high wetting ability, penetrates via open, so-called «transport», pores into the carbon material to a depth of 10 – 15 mm. Thus, the actual contact area is increased tens or even hundreds of times. This unprecedented possibility of producing electric contacts with the actual contact area of not only equal to that in the welded contact, but also larger than the rated one, is offered by a porous carbon material. But, as it is often the case in nature, positive properties are complemented by negative ones, i.e. the carbon material enters into reaction with carbide-forming components of the alloy to form at the «carbon material–metal» interface the so-called reaction layer which consists of complex carbides. As a result, the ECP surface is always covered by a carbide film, which shows up in a metallographic section as a thin interlayer of carbides. Although carbides of transition metals are electronically conducting, their resistance is always higher than that of the corresponding metals. Carbide of such an element as silicon, which is inexpensive and readily available, has a very high electrical resistance. As a result of action of these two opposing factors, the specific surface resistance (per 1 cm^2) of the welded contact at room temperature is not much lower than that of the clamping copper–graphite contact, although it remains almost unchanged during the entire service period between overhauls.

Measurements of electrical resistance of welded contacts in cathode units and graphitized electrodes, made at the «Ukrainian Graphite», showed [3] that an increase in temperature led to an increase of 20 – 25 % in resistance of the welded electric contacts. This favourably distinguishes the welded contacts from the clamping ones. Minimum electrical resistance falls exactly on working temperatures of the contact.

At the same time, electric contacts, for which the outside (surface) cooling is used, cannot be regarded as fit for long-time operation. The scale formed on the mating surfaces due to evaporation of water, which fills out pores in the electrodes, causes an increase in electrical resistance of the contact and thus leads to electric power losses. In addition, open showering of the electric contacts has a destroying effect on the furnace lining, negative effect on the ceiling structures and leads to violation of the sanitary regulations. For this reason, further steps were aimed at development of the closed water-cooled electric contacts (see Figure 5). This design of the electric contacts is characterized by the following advantages: it prevents harmful effect of water scale on the contact connections and graphite, performs compensating functions in heat variations, eliminates release of moisture into the workshop atmosphere and any unfavourable effect on the furnace lining, and it is more fit for automatic monitoring of the cooling system operation.

As was noted above, welded contacts made from the special aluminium-based electric-contact alloy allowed us to replace copper busbars of the furnace short circuit by aluminium ones. Note that aluminium is absolutely unsuitable for making clamping contacts with carbon materials operating at increased temperatures.

For assembly welding of the short circuit of aluminium busbars, the PWI developed the special semi-automatic device PSh107VA. The device can weld both aluminium thick plates to each other and aluminium compensators 9 mm in diameter to the busbars. Owing to a number of original ideas the design of the semi-automatic device is based on, it was possible to produce pore-free welds and also achieve high electrical conductivity of welded joints. This device can also be used for arc cutting of aluminium busbars.

The second challenge in terms of power saving the PWI is starting now to handle is development of the cardinally new design of the short circuit of the graphitizing furnace to ensure a drastic decrease in its reactive losses.

Therefore, completion of the entire package of the work (design of the short circuit, carbon material–aluminium welded contacts, assembly welding of short circuits of the aluminium busbars) will provide a fundamental saving of power resources. According to our estimates, reactive losses will be decreased by 20 % of the absolute ones and active resistance of the short circuit will be decreased by 10 %, which will provide a reduction in the specific power consumption of 45 – 500 kW·h per each ton of the graphitized electrodes.

It should be noted in conclusion that results of the work done by the PWI by request of the Company can be utilized also by other industrial enterprises which use electrometallurgy plants with high-power electric contacts between carbon materials and metals operating at increased temperatures.

REFERENCES

1. Chalykh, E.F. (1972) *Technology and equipment of electrode and electric-carbon enterprises*. Moscow: Metallurgia.
2. Lakomsky, V.I. (1995) Open-arc welding of carbon materials to metals. *Avtomaticheskaya Svarka*, **8**, 11 – 18.
3. Lakomsky, V.I. (1998) Welded electric contacts «carbon material–metal» in non-ferrous metallurgy plants. *Ibid*., **2**, 18 – 32.
4. Lakomsky, V.I. (1997) *Oxide cathodes of the electric arc*. Zaporozhie: Integral.

TECHNOLOGY OF ELECTRON BEAM WELDING OF HIGH-STRENGTH ALUMINIUM ALLOY STRINGER PANELS

A.Ya. ISHCHENKO, A.A. BONDAREV, S.V. NAZARENKO and **Andr. A. BONDAREV**
The E.O. Paton Electric Welding Institute, NASU, Kyiv, Ukraine

ABSTRACT

Comparative estimation of methods of manufacture of light stiffened panels of aluminium alloys is shown. Advantages of the electron beam welding process for manufacture of thin-walled panels from high-strength heat-hardened aluminium alloys are given. Technology of a single-sided welding of stiffeners of thin sheets and plates at ratio of thicknesses from 1:1 to 1:15 and higher is developed. It was established that the programmed heat input within the circuit of the electron beam scanning during welding is the most effective means of control of weakening and shape of penetration zone of T-joints.

Key words: *electron beam welding, scanning with a beam, aluminium alloys, stringer panels, stiffeners, weakening zone,* T*-joint, programming of heat input.*

In manufacture of different-purpose aluminium structures the thin-walled panels with a set of stiffeners are used. The application of high-strength aluminium alloys for this purpose promotes the significant reduction in their mass while the high values of strength and rigidity are provided.

In production of stiffened panels made from aluminium alloys, a technology of hot pressing, in which nonheat-hardenable aluminium alloys are mainly used, found a wide spreading. In case of using heat-hardened aluminium alloys the stiffened panels are manufactured by a mechanical or chemical milling. Both these methods have a number of essential drawbacks. The first method is characterized by impossibility of producing panels in a cold-worked or heat-treated state that reduces their strength characteristics. The second method is characterized by a low metal utilization factor, a low productivity and a high cost [1].

On this basis the different versions of joining stiffeners to a sheet were developed using welding. Work [2] describes the diffusion welding of such structures. This method of joining has a number of limitations, one of which is associated with a difficulty in producing panels of large sizes. Twin-arc argon welding into a common pool found the wider application [3, 4]. However, in this case, when using small thickness of a stiffener and panel (1.5 – 3.0 mm) a HAZ is propagated across their thickness and the residual welding deformations have inadmissible sizes.

The manufacture of large-sized stiffened panel by an electron beam welding (EBW) seems to be promising. The application of the EBW widens the range of thicknesses of a sheet and stiffeners, promotes the use of high-strength and hard-to-weld aluminium alloys without a noticeable their weakening in the weld zone, and, most importantly, such panels have comparatively small deformations. Welding can be performed both from the side of a stiffener [5] and also from the side of a sheet [6] depending on a design peculiarities and technological capabilities of the equipment.

The welding of a stiffener with two fillet welds using an electron beam, as described in [5], provides not only the minimum HAZ and reduction in residual welding deformations, but also a high accuracy in assembly due to a preliminary elastic tension of a sheet and stiffeners to be welded. However, it should be noted that the design of a stand for the pretension is a rather complex and metal-intensive structure that complicates the technological process and influences the cost of the products.

The present work is aimed at searching the ways of improving the technology of manufacture of welded stiffened panels, evaluation of different versions of producing T-joints with an electron beam (single- or double-sided welding of a stiffener, making of a slot weld), optimization of welding parameters with a heat input programming [7], and also at reduction of residual welding deformations and weakening of the high-strength alloy parent metal in the weld zone at the expense of using massive heat-dissipating devices and reverse bending of the panel before welding [8].

Welding of mock-ups was performed in installation U-212M (power source U-250A, 60 m/h speed and 30 kV accelerating voltage). The beam displacement was controlled in different paths and the heat input was programmed with the help of SU-261 instrument. Sheets and stiffeners of the

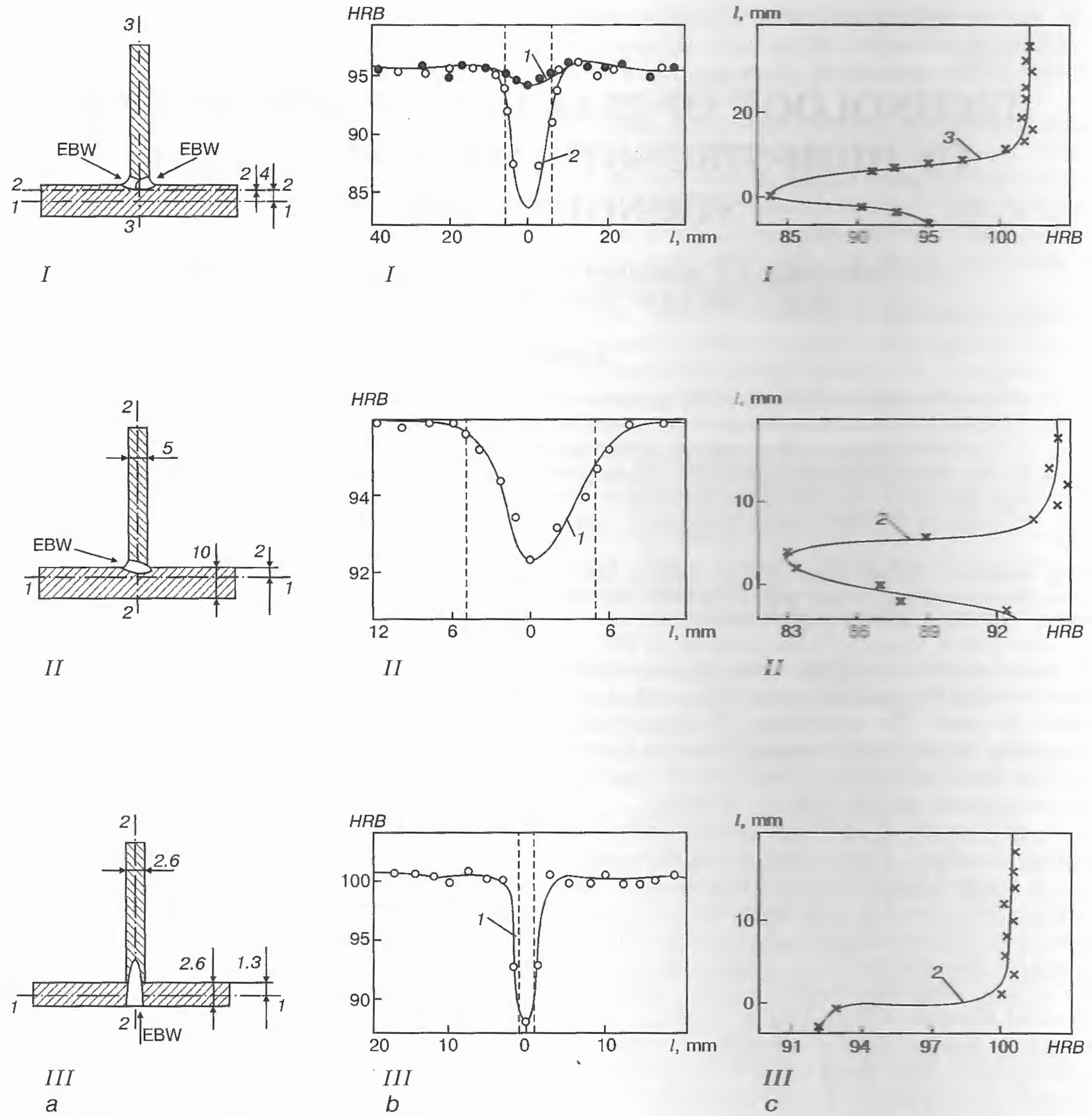

Figure 1. Distribution of hardness in the zone of welding: *a* — versions of welded joints of a thin-walled stiffener with a sheet in manufacture of stringer panels; *b* — distribution of hardness in the zone of a sheet welding; *c* — the same, in the zone of a stiffener welding; *I*, *II* — double- and single-sided weld on alloy AMg6N, respectively; *III* — slot weld on alloy D16; figures *1* – *3* denote curves of hardness changes

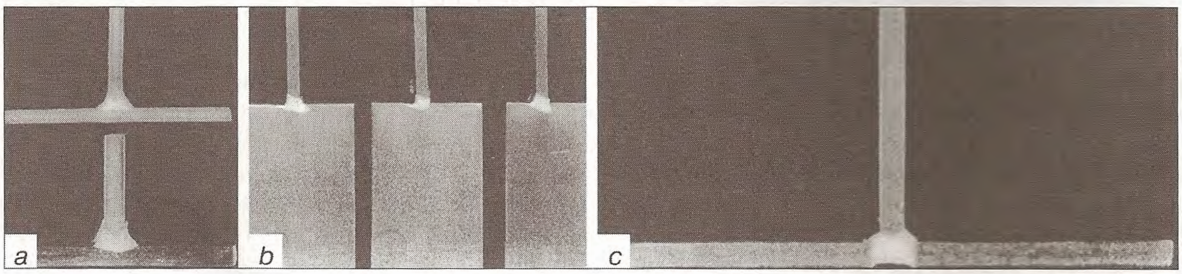

Figure 2. Macrosections of T-joints of aluminium alloys: *a* — double-sided weld on alloy 1430 with 2.8 mm thickness of elements; *b* — single-sided weld on alloy 1423 with 1.8 and 35.0 mm thickness of elements; *c* — slot weld on alloy D16 with 2.4 mm thickness of elements

mock-ups of panels were manufactured from aluminium alloys of AMg6N, 1423, 1430 and 1460 grades. Alloy AMg6N was selected due to its highest susceptibility to weakening under the action of the welding thermal cycle, and the heat-hardenable aluminium-lithium alloys of 1423, 1430 and 1460 grades were selected as most promising for the manufacture of light structures of different purposes, including the aerospace engineering.

To decrease the residual welding deformations the panels were welded on a massive heat-dissipating assembly stand at a tight pressing of the panel all over the surface. To compensate the angular deformations the assembly stand was manufactured from a special shaped section that ensures a reverse bending of the panel sheet during assembly before the welding of stiffeners.

The sheet with stiffeners was welded with two fillet welds made successively from two sides of the stiffener or with one fillet weld with a through penetration of the stiffener across the whole thickness for one pass. In the third case the stiffener was welded with a slot weld for one pass through the sheet body (Figure 1). To ensure a complete fusion of the stiffener edge in a double-sided welding the angle of beam inclination to the panel was varied in the range of 45 – 20°. It was established that the overlapping of welds at stiffener thickness from 2 to 5 mm occurs at the 25 – 30° angle of beam inclination and minimum penetration in the panel depth.

To guarantee the stiffener edge fusion across the whole thickness in a single-sided welding, the angle of beam inclination was varied in the range of 10 – 25°. At the stiffener thickness of up to 5 mm the optimum angle of beam inclination was 20°. Welding of T-joint with a slot weld was performed by a beam scanning with an amplitude, equal to the stiffener thickness, and by using a filler in the form of embedded elements between the stiffener and panel to provide a complete fusion of the stiffener edge and formation of fillets in the joint corners.

Figure 2 presents the results of determination of a degree of weakening of the parent metal from the hardness measurement in two planes: in a stiffener axis and in the middle part along the sheet plane. As is follows from the Figure, the parent metal weakening to the level of the as-annealed state occurs during the double-sided welding of alloy AMg6N directly under the stiffener at the 2 mm depth. The total width of the weakening area is about 20 mm. The stiffener is weakened approximately for a half of this size starting from the sheet surface. However, at the 4 mm distance from the sheet surface directly under the stiffener the decrease in parent metal hardness is negligible. Thus, if the thickness of the panel sheet is twice larger than that of the stiffener, then the complete weakening of the sheet under the stiffener will not occur even in case of deposition of double-sided welds. It should be noted that at such scheme of making T-joints the level of residual deformations was higher than admissible values because of a large volume of remelted metal.

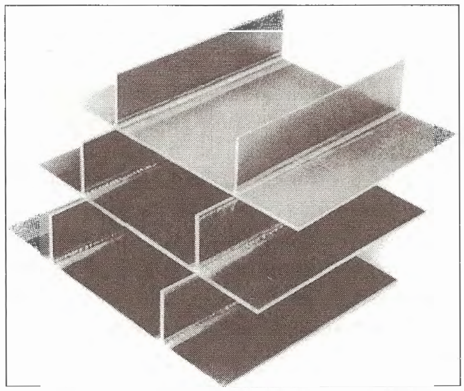

Figure 3. Appearance of fragments of welded stringer panels from aluminium-lithium alloys of 1460 grade (2.2.mm thickness) and 1430 grade (2.8.mm thickness)

In single-sided welding of the same joint directly under the stiffener the complete weakening was not observed even at the 2 mm depth from the sheet surface, and the total width of the zone of a partial reduction in hardness of the parent metal of the sheet is only 10 – 12 mm. In the stiffener body the weakening zone does not exceed 10 mm. Due to the fact that at such scheme of welding the shrinkage is observed only in one plane, i.e. along the stiffener axis, the residual deformations are minimum.

In welding T-joints with slot welds the hardness of the sheet material directly under the stiffener corresponds to the that of the cast metal. The above-mentioned scheme of the joint making is not very promising, if it is necessary to preserve the strength properties of the parent metal at the higher level. Moreover, here the residual angular deformations have comparatively high values.

As the angular and longitudinal deformations depend on the sizes and shape of the penetration zone, attempts were made in our investigations to optimize these parameters of the weld. For this purpose, the technology of welding with a discrete-scanning beam and heat input programming within the heat spot was used. The control of time of beam delay in the discrete points could avoid the formation of root defects in making both the fillet and slot welds, that was established from the results of 100 % X-ray examination of the welded specimens. This was also proved by macrosections of T-joints of alloys of 1430, 1423 and D16, which are sensitive to the formation of root defects in the conditions of a partial penetration (Figure 2). As the experiments showed, the scanning trajectory (circle, with a higher heat input in the lateral sides of the weld), 1000 Hz frequency, 2.0 – 2.5 mm amplitude can be assumed to be the optimum parameters.

The use of the results of investigations, and also the equipment developed allowed welding of specimens of stringer panels from aluminium-lithium alloys of 1460 and 1430 grades to be performed at 2.2 and 2.8 mm thickness of elements to be welded, respectively (Figure 3). As the data of next micrometric area of panels showed, the residual deformations were within the admissible values in spite of very small thickness of sheets and stiffeners being welded.

REFERENCES

1. (1980) *Special-purpose shaped sections from aluminium and magnesium alloys.* Handbook-Catalogue. Ed. by M.Z. Ermak. Moscow: Metallurgia.
2. Gelman, A.A., Kolodkin, A.I., Pavlov, V.M. *et al.* (1978) Diffusion welding of T-joints from titanium alloy VT6S. *Svarochnoye Proizvodstvo*, **5**, 15 – 17.
3. Zhukov, M.B., Karasyov, L.V., Vakutinsky, M.M. *et al.* (1978) Technology of manufacture of welded stiffened panels from sheet and pressed prefabrications. *Ibid.*, **2**, 50 – 51.
4. Zhukov, M.B., Penchuk, P.N., Redchits, V.V. *et al.* (1987) Double-sided welding of T-joints with two arcs in a common pool. *Avtomaticheskaya Svarka*, **7**, 46 – 48.
5. Paton, B.E., Lobanov, L.M., Pavlovsky, V.I. *et al.* (1989) Manufacture of welded large-sized thin-walled panels from high-strength aluminium alloys. *Ibid.*, **10**, 37 – 46.
6. Slivinsky, V.A., Shevelev, A.D., Zamkov, V.N. *et al.* (1989) Electron beam welding of elements of stiffened panels from titanium alloy VT-20. *Ibid.*, **4**, 55 – 57.
7. Lankin, Yu.N., Bondarev, A.A., Baishtruk, E.N. *et al.* (1985) Control of distribution of electron beam power density in its section. *Ibid.*, **6**, 12 – 15.
8. Bondarev, A.A., Nazarenko, S.V., Bondarev, Andr. A. (1999) Improvement of technology of manufacture of welded stiffened panels from high-strength aluminium alloys. In: *Proc. of IV Int. Sci.-Techn. Conf. on Problems of Welding, Metallurgy and Allied Technologies*, Tbilisi, Oct., 1999. Tbilisi.

REDUCTION OF METAL SPATTER IN CONSUMABLE-ELECTRODE WELDING IN CO_2

P.P. SHEIKO, A.M. ZHERNOSEKOV and **S.A. SHEVCHUK**
The E.O. Paton Electric Welding Institute, NASU, Kyiv, Ukraine

ABSTRACT

New approach to the solution of problem of a spattering decrease during CO_2 welding is suggested. It consists in the fact that short circuits are created continuously with the help of electronic methods according to a preset program. A pilot model of the welding equipment using IGBT transistor is manufactured. The application of the mentioned approach allows the metal spattering to be decreased by 40 – 50 %.

Key words: *consumable electrode welding, shielding gases, spatter, metal transfer control.*

Mechanized arc welding in CO_2 with solid electrode wire is widely accepted in welding production in fabrication of metal structures of carbon and alloyed steels. Despite a number of disadvantages (higher spatter of electrode metal and unsatisfactory weld formation) this method is one of the leading mechanized arc welding processes in terms of both the volume of metal structures made and the number of the operating units and workers employed.

Development of argon-based oxidizing gas mixtures over the recent decades, enabled many problems of electrode metal transfer to be solved and its spatter to be reduced [1 – 3]. The consumption and cost of welding consumables, however, become much higher in this case. Thus, development of the new techniques of reduction of metal losses for spatter in CO_2 welding with solid electrode wire is still urgent nowadays.

Electrical engineering and physico-metallurgical techniques are used in order to eliminate the above shortcomings. The first are related to control of the welding current shape at different stages of formation and growth of the drop at the electrode tip, as well as its transfer into the weld pool [4]. The second envisage addition of easily-ionized alkali and rare-earth elements into the electrode wire [5, 6].

Note that in the first case, development of power sources with a controlled shape of welding current requires complex microprocessor control with several feedback channels by different parameters of the welding process. This, in its turn, predetermines a relatively high cost of welding equipment and high qualifications of personnel for optimization of the technology of welding and servicing the equipment [7].

In the second case, the problem of spatter reduction in CO_2 welding is solved at the expense of application of costly activating components and special technology of production of activated welding wires.

It is known that the process of CO_2 welding at medium currents is characterized by globular transfer of the metal, arc erring over the drop surface, which, in combination with many other force factors active in the welding arc zone, leads to short-circuiting of the arc gap, breaking up of the liquid bridge between the electrode and the weld pool. The concurrent electric explosion and gas-dynamic impact promote a greater spatter of the metal.

The approach suggested by us consists not in detection of the chaotic, spontaneous short-circuits, but in their systematic generation by electronic methods by a preset program. More over, it is necessary to satisfy such a condition — the diameter of the forming drops should not exceed approximately 1.2 to 1.4 electrode diameters. Otherwise, the spatial displacements of large drops can give rise to random instantaneous short-circuits at the electrode tip with drop rejection beyond the weld. The ratio of the number of such instantaneous short-circuits caused by large drops with spattering to their total number is up to 2.5 to 3.1 [8]. Shorting of the slightly melted electrode and control of the short-circuiting current will enable a smooth transition of the drop into the weld pool as a result of the combined impact of the surface tension forces and actively controlled electromagnetic forces. The recently developed controlled semi-conductor devices allow the suggested approach to be implemented.

Figure 1 gives the functional diagram of the pilot sample of welding equipment used to study the technological capabilities of the proposed technique of CO_2 welding. The welding current source (*CS*) is the multi-purpose rectifier I-187 developed in the E.O. Paton Electric Welding Institute. The base current for maintaining the arcing in the ab-

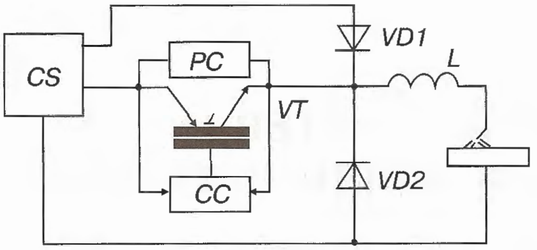

Figure 1. Block diagram of a pilot sample of the welding unit

sence of the force pulses, is provided by the appropriate windings of the source. The base current circuit is connected to the welding arc through diode *VD*1 in the point of connection of diode *VD2* and welding choke *L*. The amplitude value of the current pulses is assigned by I-187 source. Transistor *VT* serves for generation of the current pulses of the required shape, as well as limiting the short-circuit current to the required level. The control circuit (*CC*) generates controlling pulses which set the required algorithm of the transistor operation.

Since transistor *VT* is an IGBT transistor, i.e. an actually variable transistor controlled by input voltage, there is a possibility without current feedback, to perform the required limitation of current in the welding circuit at a specified level. The control circuit traces the start of the current pulse. The control signal (Figure 2) at the initial moment of the force pulse, is fed with U_{lim} amplitude which limits the transistor conductivity and, therefore, the current in the welding circuit to a required level. After a certain interval of time $(t_1 - t_2)$ experimentally established to be $(1 - 2)\cdot 10^{-3}$ s, the control signal reaches the value of U_w necessary for a complete unblanking of the transistor.

In view of the above, current limitation occurs only at the moment of its rise and resulting drop separation. Several measures are built into the circuit in order to prevent the emergency situations. Diode *VD2* limits the pulsed increase of back voltage on *VT* transistor induced in the welding circuit by choke *L* at the expense of self-induction at current lowering. Protection circuits (*PC*) prevent the appearance of catastrophic overvoltages on transistor *VT* during the rise and drop of current in the circuit. Reduction of the rise of voltage applied to

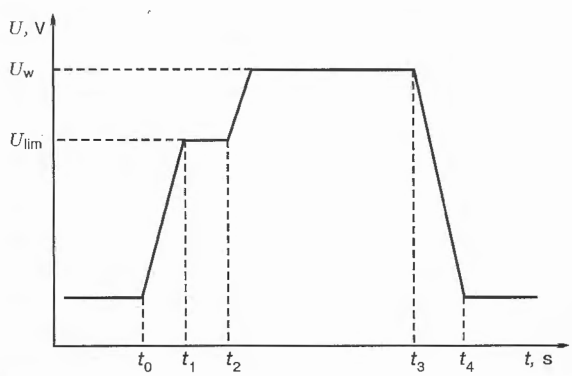

Figure 2. Shape of the control signal

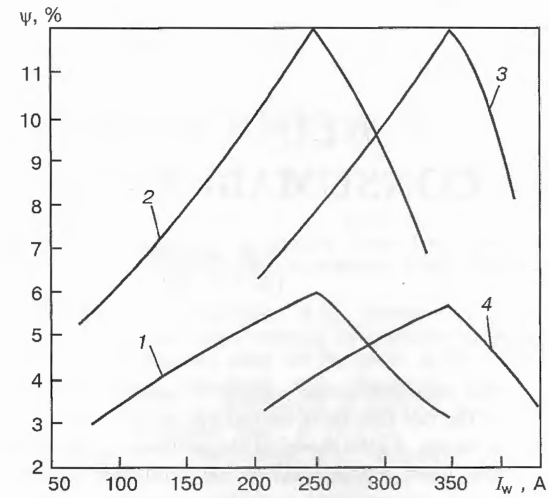

Figure 3. Dependence of the coefficient of electrode metal losses for spatter and burning out on welding current: *1, 4* — new welding technique; *2, 3* — existing technology; *1, 2* — use of welding wire of 1.2 mm dia.; *3, 4* — the same of 1.6 mm dia.

the transistor is further promoted by feeding control pulses with rated fronts of rise $(t_0 - t_1)$ and drop $(t_3 - t_4)$, i.e. the current rise and drop proceed during a quite considerable time interval (approximately $1\cdot 10^{-3}$ s).

The control circuit traces the level of power evolving in the transistor at the moment of current limitation. In the case if the power values indicated in the certificate are exceeded, the control signal is cut off and the transistor is switched off. Such power monitoring occurs at the moment of the current pulse passage and is performed by «saturation», i.e. if the voltage drop on transistor *VT* at the moment of current passage exceeds a certain value, the transistor is switched off, thus eliminating its overheating or malfunction as a result of the thermal break through. Diode *VD1* is used to prevent blanking of the base current source by the pulse current source.

The unit the functional diagram of which is given in Figure 1, operates as follows. A current pulse is passed through the arc, its amplitude and duration being assigned so as to form a drop of not more than 1.2 to 1.4 diameters of electrode wire at the electrode tip. Then, the current pulse is reduced to the values of pause current of 20 to 50 A. Under the action of the gravity forces with insignificant electromagnetic forces, the drop is hanging down. In the next moments of the pause, the drop, as a result of the electrode wire feed, bridges the arc gap, merging with the molten metal of the weld pool. The drop metal is pulled down into the pool by the surface tension forces. This is followed by a current pulse which due to rising electromagnetic force, causes breaking up of the bridge already formed by the surface tension forces and noticeably thinned to minimal diameter and volume. In this case the current does not rise above the specified value due to the features of IGBT transistor. Such

Welding current, A	*Arc voltage, V*	*Wire feed rate, m/h*	*Welding speed, m/h*	*Coefficient of losses (proposed technique), %*	*Coefficient of losses (GOST 25616–83), %*
100 – 110	20 – 21	240	7	3.4	6
150 – 160	22 – 24	390	11	4.6	8
180 – 190	25 – 26	535	12	5.0	10
250 – 260	26 – 28	710	15	6.0	12

Note: In all the cases, the voltage of the pulse current generation is 71.5 V, that of the base is 42.5 V.

conditions permit the drop to smoothly run into the weld pool without explosion of the bridge, thus reducing the spatter.

The Table systematizes the results of experimental studies of the influence of the proposed technique of reduction of the metal losses for spatter and burning out in bead deposition on plates of 09G2 steel 8 mm thick with Sv-08G2S welding wire of 1.2 mm diameter. The welding process parameters were selected to achieve minimal spatter and optimal formation of the weld metal. The voltages at which the pulse and pause currents were generated, were the same in all the experiments. The welding current and arc voltage were adjusted by the electrode wire feed rate.

Figure 3 shows the dependencies of the coefficient of metal loss for spatter and burning out on welding current for wires of 1.2 and 1.6 mm diameter. A lowering of metal losses for spatter and burning out by 40 to 50 % is achieved in the entire range of welding currents, compared to standard values (GOST 25616–83).

It should be noted that inexpensive mobile attachments to the available series-produced welding arc power sources can be developed, in order to implement the proposed technique.

Thus, the proposed technique of reduction of metal spatter in consumable-electrode welding in CO_2, enables a significant (up to 50 %) reduction of metal losses. This is achieved due to such control of the processes of melting and transfer of electrode metal in which an ordered systematic transfer of the drops of the size of not more than 1.2 to 1.4 electrode diameters takes place, with limitation of the short-circuit current and abrupt reduction of the energy of the bridge explosion, as well as elimination of the instantaneous random short-circuits and of the electrode metal spatter caused by them.

REFERENCES

1. Killing, R. (1983) Schutzgase zum Lichtbogenschweissen. *Praktiker*, **6**, 326 – 330.
2. Sroka, V., Winkler, R. (1994) Mischgase zum MAG-Schweissen von Stahlen. *Schweisstechnik*, **10**, 148 – 154.
3. Steidl, L. (1992) Schweissen von Maschinenrahmen im TIEM-Prozess. *Ibid.*, **12**, 201 – 204.
4. Paton, B.E., Lebedev, A.V. (1988) Control of melting and transfer of electrode metal in CO_2 welding. *Avtomaticheskaya Svarka*, **11**, 1 – 5.
5. Paton, B.E., Voropai, N.M. (1979) Gas-shielded welding with activated metal electrode. *Ibid.*, **1**, 1 – 7, 13.
6. Voropai, N.M., Lavrishchev, V.Ya. (1976) Conditions of electrode metal transfer in CO_2 welding. *Ibid.*, **5**, 8 – 11.
7. Stava, K. A (1993) New low-spatter arc welding machine. *Welding J.*, **1**, 25 – 29.
8. Shuyian, Y., Zheng, G. (1994) Effect of arc physics on developing of CO_2 arc welding. *China Welding*, **1**, 1 – 9.

NEW METHOD FOR THE MANUFACTURE OF THERMOCHEMICAL CATHODES FOR PLASMATRONS

V.V. ARSENYUK
The E.O. Paton Electric Welding Institute, NASU, Kyiv, Ukraine

ABSTRACT

Results of investigations on vacuum percussion welding of zirconium and hafnium to copper for the manufacture of thermochemical cathodes for plasmatrons are given. Thechnological parameters of welding and forming of parts are determined. The technology and equipment developed for the manufacture of four types of the thermochemical cathodes are described. The new method for the manufacture of the thermochemical cathodes allows substantial saving of scarce metals, improvement in reliability and extension of service life of plasma installations.

Key words: *percussion welding, thermochemical cathodes, technology, plasmatron, erosion tests.*

Air-plasma cutting of metals is widely applied in many industries. Development of new designs of plasmatrons involves an intensive search for materials for making components of the thermochemical cathodes and methods for their joining to improve technical characteristics of plasma installations.

Thermochemical cathodes of plasmatrons should ensure sparing consumption of the electrode material, stability of the arc discharge in an oxygen-containing atmosphere and high productivity.

Zirconium and hafnium electrodes fixed in a water-cooled copper casing of the cathode meet all these requirements [1]. Comparative tests of zirconium and tungsten electrodes conducted at a working current of 500 A and air flow rate of 350 m^3/h show that erosion resistance of the zirconium electrodes is 50 – 70 times higher than that of the tungsten electrodes. Such a high resistance of the zirconium electrodes and excellent emission properties of the zirconium cathode are attributable to the fact that zirconium oxides and nitrides formed at the surface of the electrode tip during the arc discharge do not only protect the electrode material from burning out in air, but, what is more important, they maintain the stable arc discharge.

The trend to increase in the arc current to 1000 A and more made it necessary to develop special zirconium-based metal-ceramic electrodes alloyed with rare-earth and other elements [2, 3].

However, high values of service characteristics of the cathodes depend not only upon the electrode material. The manufacture technology has a much higher impact than chemical composition of the cathodes.

The most widespread method for making thermochemical cathodes is pressing-in of the electrode material into the copper casing, which provides a tight fit between the electrode surface and the copper casing. However, defects in the form of pores, gaps, oxide inclusions, etc. might be present in a thermochemical cathode along the line of contact. This causes a drastic decrease in thermal and electrical conductivity and reduction in life of parts.

One of the promising areas that offer an extension of life of the thermochemical cathodes in plasmatrons is welding of a zirconium or hafnium electrode to a copper casing. As zirconium and hafnium, when joined to copper, are characterized by a limited mutual solubility in the solid state, during heating they form intermetallic compounds and eutectics. Joining these metals involves difficulties, while it is almost impossible to joint them by fusion welding. Therefore, the only method that holds promise for these metals is solid-state joining.

The work described in this article was aimed at development of the technology and equipment for making welded thermochemical cathodes with improved performance.

The new method for solid-state joining, i.e. vacuum percussion welding, was used for this purpose [4]. The main point of this method is that single loading pulses are applied at a rate of 1 to 30 m/s to the locally heated regions within the joining zone.

Main parameters of the process of vacuum percussion welding include heating temperature and impact energy. The latter provides the required high-rate deformation of the contact zones of the metals joined. Vacuum percussion welding is done using a machine which consists of a work chamber with a mechanism for applying the impact load to the parts joined, power supply and control panel. The work chamber (Figure 1) houses an electron beam heater which moves along the length of the parts joined. It allows the temperature of the metal within the joining zone to be brought to a desirable level during heating.

The cycle of percussion welding comprises several stages: preparation, welding and cooling.

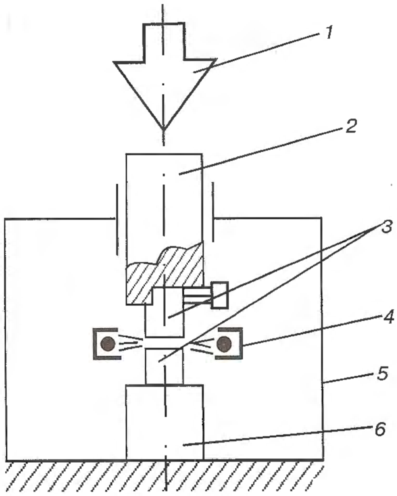

Figure 1. Schematic of vacuum percussion welding: *1* — striking pin; *2* — rod; *3* — samples joined; *4* — annular electron beam heater; *5* — vacuum chamber; *6* — anvil block

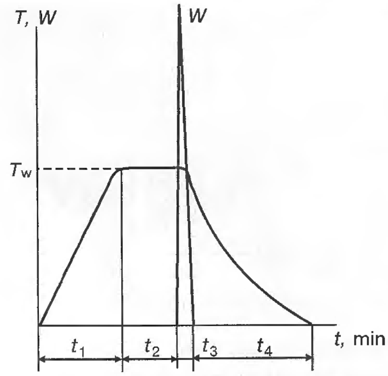

Figure 2. Cyclogram of the percussion welding process: T — preheating temperature; W — impact energy; t_1, t_2, t_3 and t_4 — time of heating, respectively, to T_w, holding at T_w, the welding process $(1{\cdot}10^{-2} - 1{\cdot}10^{-3}$ s) and cooling

Preparation for welding includes preheating of a part to the welding temperature, holding at this temperature to ensure uniform heating of the parts within the joining zone (Figure 2) and cleaning them from oxides (like in the case of auto-vacuum welding).

Welding of copper to zirconium or hafnium, which substantially differ in physical-chemical and mechanical properties, is done using a special device to ensure a uniform directed deformation of metals within the joining zone at the moment of impact by the dynamic load.

The device consists of a die which, prior to welding, fixes the metals to be joined over the forming channel [5]. After the parts are heated to a welding temperature and held at the constant values of T_W, a loading pulse is applied to them to cause movement of the heated parts to the forming chamber. Joining of copper to zirconium occurs in the chamber within $1{\cdot}10^{-2} - 1{\cdot}10^{-3}$ s, then follows an intensive cooling of the welded joint.

Comparative study of the rate of cooling of the samples welded with and without the forming die shows that in the former case it is 6 – 7 times higher (Figure 3).

Samples of copper M1 were welded to zirconium or hafnium. Welding was done under the following conditions: $T_W < (0.8 - 0.9)T_{eut}$, where $T_{eut} = 710 - 795$ °C is the temperature of the lowest melting point eutectic in the copper-zirconium system. The specific surface impact energy was 100 – 200 J/cm^2.

Standard specimens with a diameter of 3 mm were cut out from the welded samples for mechanical tensile tests. Strength of the joints between zirconium and copper (Table) welded at a preheating temperature of 750 – 780 °C and specific impact energy of 170 J/cm^2 is at a level of tensile strength of copper (σ_t = 220 – 250 MPa).

It follows from analysis of the mechanical tests and metallography results that the optimal temperature of preheating is 750 – 780 °C. Rapid deformation and cooling of the samples welded in a cold forming die create conditions for the formation of a strong joint, containing no low melting point eutectics and intermetallics (Figure 4, *a*). Low strength of the welded joints made at a preheating temperature of 650 – 700 °C is attributable to an insufficient intensity of thermochemical activation of the welding process, while at a temperature above 800 °C the effect of the dynamic loading pulse is accompanied by an increase in the heating temperature. In turn, this leads to the formation of the eutectic centres within the joining zone. This is evidenced by the metallography results (Figure 4, *b*).

A new method for the manufacture of thermochemical cathodes was suggested on the basis on

Mechanical properties of the copper-zirconium welded joints depending upon the welding temperature (specific impact energy — 170 J/cm^2)

Welding temperature, °C	σ_t, *MPa*	δ, %	*Fracture*
650 – 700	< 150	–	Joint
750 – 780	220 – 250	60	Base metal
800 – 850	< 50	–	Joint

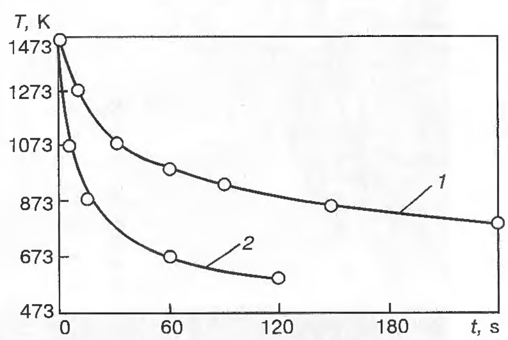

Figure 3. Variation in temperature of the copper-zirconium welded samples during cooling: *1* — diagram of free deformation; *2* — using cold forming devices; *t* — time of cooling of a part

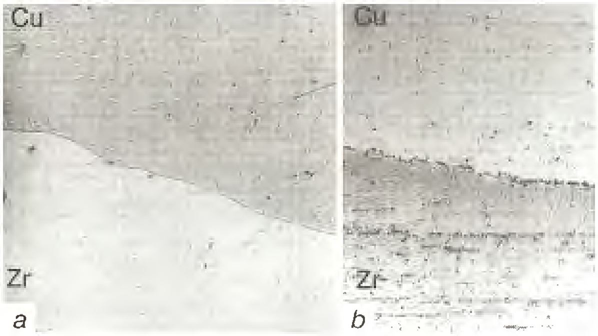

Figure 4. Microstructures of the joining zones between copper and zirconium formed in percussion welding at T_w, °C: *a* — 750 – 780; *b* — > 800 (×200) (reduced by 0.80)

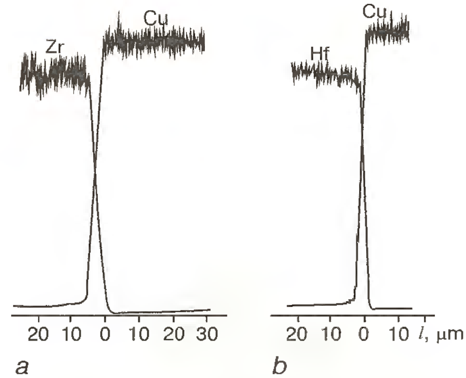

Figure 5. Distribution of elements in the joining zone: *a* — copper–zirconium; *b* — copper–hafnium; *l* — distance from the contact line

the investigations conducted. The method combines solid-state joining and forming, using specialized devices characterized by a strain rate above $1 \cdot 10^2$ s^{-1}.

High strain rates within the zone of contact of copper and zirconium favour the formation of an active electrode insert (zirconium) in the form of a short cylindrical rod with a neck. This shape has a high practical advantage over others which may be formed in the manufacture of thermochemical cathodes by the method of pressing-in, in terms that the above shape promotes decreasing the stressed state of the joining zone and thus helps eliminate destruction of the thermochemical cathode during operation.

Metallography of the joining zone formed in percussion welding under optimal conditions shows that the zone between the zirconium or hafnium electrode and copper casing contains no defects in the form of discontinuities, gas bubbles extended along the interface or endogenous inclusions (eutectics, intermetallic or other compounds).

Analysis by the radiographic, spectral electron-diffraction and electron probe *X*-ray methods indicates that the joining zone between the electrode and copper casing consists of solid solutions of both copper in zirconium and zirconium in copper (Figure 5).

Investigation of a microstructure of the joining zone evidences that shear deformations lead not only to a displacement of microvolumes of the active insert material (zirconium) into copper, but also cause shear of the surface layers of zirconium and their movement into copper in a direction of the electrode axis during the forming process (Figure 6). The experimentally found effect of displacement of the surface layers is indicative of the fact that the decisive role in the formation of a welded joint during percussion welding in vacuum is played by a directed shear deformation.

A strong joint in vacuum percussion welding is formed in the case where sufficient tangential stresses result in a substantial plastic strain in the subsurface layers, accompanied by movement of a large number of dislocations. The investigation results suggest that the process of vacuum percussion welding combined with forming occurs under conditions close to adiabatic, which favours an increase in plastic flow of metals within the joining zone.

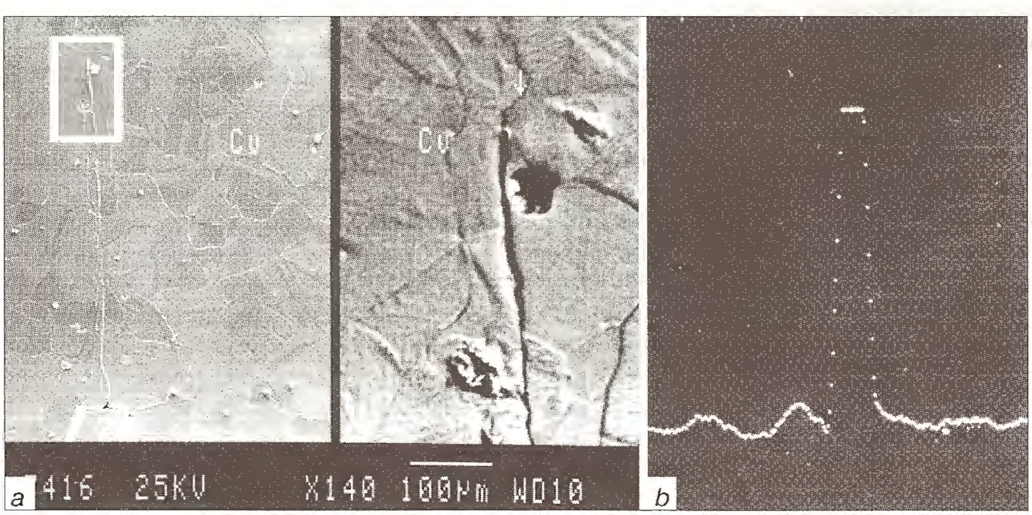

Figure 6. Distribution of zirconium in copper: *a* — microstructure of the joining zone; *b* — distribution of zirconium in a marked region (reduced by 0.80)

The investigations show that the temperature of preheating for the pairs of metals under consideration should be 100 °C lower than the eutectic formation temperature.

Thermochemical cathodes of plasmatrons were tested using a special rig under the following conditions:

arc current, A .... 250 – 300
arc voltage, V .... 150 – 170
duty cycle, s 60
time of pause, s 5

The characteristic curve shown in Figure 7 illustrates dynamics of burning out of the hafnium electrode, which is similar to that when using the zirconium electrode. However, the number of turnings on is approximately 250 for zirconium and 450 – 500 for hafnium. In addition, as shown by the test results, the welded thermochemical cathodes are characterized by a stable service life, which is 1.5 – 2.0 times longer for all of the samples tested, as compared with the pressed-in zirconium and hafnium electrodes of [6].

Analysis of the curve of dynamics of burning out of the electrodes shows that this curve has certain characteristic regions. An increased rate of erosion of an electrode at the initial period of the tests is likely to be associated with the presence of lack of penetration, 0.5 – 1.0 μm long, in the edge porion of the joining zone between the copper casing and active zirconium insert, formed as a result of constrained conditions of deformation of the metals joined in a cold die. Further tests revealed a moderate consumption of the electrode material. Metallography of the thermochemical cathodes, conducted after the test cycle, detected no intermetallic compounds, eutectics and defects.

It was established that during the erosion process the characteristic zones of the crater did not differ in chemical composition or properties from those of the thermochemical cathodes made by the method of conventional pressing in of the electrode material. The characteristic feature of erosion of the electrode in the thermochemical cathode produced by percussion welding is the formation of an intermetallic compound in the form of a sharp wedge at the ends of the crater not more than 0.2 mm deep and 0.012 mm wide. The general picture of the characteristic zones of the crater during the erosion process remains unchanged until the electrode of the thermochemical cathode is completely burnt out.

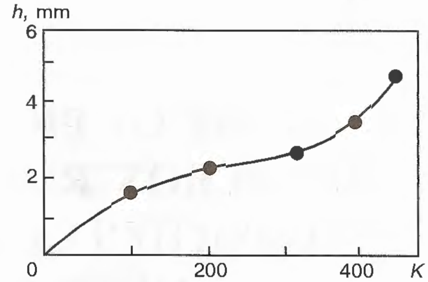

Figure 7. Depth of erosion, h, versus amount of inclusions, K

Special equipment was developed and fabricated for the manufacture of four types of the thermochemical cathodes.

CONCLUSIONS

1. The new method for percussion welding in vacuum was developed. It combines the processes of welding and forming. Optimal parameters were identified for the manufacture of four types of the thermochemical cathodes with zirconium and hafnium electrodes.

2. Welded joints between hafnium and zirconium electrodes and a copper casing of the thermochemical cathodes were produced for the first time. The joints are characterized by the absence of a layer of intermetallics or eutectics. The joining zone is the zirconium–copper or hafnium–copper solid solution.

3. The equipment and technology developed enable the annual requirement of electrodes for plasmatrons to be reduced by 20 % owing to extension of their service life, consumption of scarce materials to be decreased, and reliability and time of operation of plasma installations to be increased.

REFERENCES

1. O'Brien, R.L., Wickham, P.J., Keam, W.R. (1964) Advances in plasma arc cutting. *Welding J.*, **12**, 114 – 116.
2. Matsuda, F., Ushio, M. (1990) Comparative study of air-plasma cathode durability — new cathode materials for air. *Plasma Cutting*, **3**, 132 – 136.
3. Lakomsky, V.I. (1997) *Oxide cathodes of the electric arc*. Zaporozhie: Integral.
4. Ignatenko, A.I., Kharchenko, G.K. *Method for pressure welding*. USSR authors' certificate **404588**, Int. Cl. B 23 K 19/00. Publ. 22.10.73.
5. Ignatenko, A.I., Kharchenko, G.K., Gurienko, V.P. *et al.* (1989) Vacuum percussion welding of dissimilar metals. In: *News letter*, **7**. Series of welding equipment. Kyiv: PWI.
6. Arsenyuk, V.V., Danilchenko, B.V., Ignatenko, A.I. *et al.* (1995) Vacuum percussion welding of zirconium and hafnium to copper to manufacture electrodes for plasmatrons. In: *Proc. of «Welding-95» Russian Sci.-Techn. Conf. on Modern Problems in Welding Science and Technology. Perm.*

PACKAGE OF PROGRAMS FOR PREDICTION OF MICROSTRUCTURE AND MECHANICAL PROPERTIES OF HAZ METAL IN WELDING OF STRUCTURAL STEELS

A.F. MUZHICHENKO
The E.O. Paton Electric Welding Institute, NASU, Kyiv, Ukraine

ABSTRACT

The described software enables computation of structure and mechanical properties of the HAZ metal in welding of structural steels on the basis of $t_{8/5}$ determined from the heat models, steel grade from the computer atlas of the austenite decomposition diagrams or chemical composition of steel from the regression models.

Key words: *software package, heat model, martensite, bainite, ferrite, pearlite, Vickers hardness, tensile strength, yield strength, reduction in area at fracture, impact toughness.*

The possibility of ensuring the specified level of mechanical properties of the HAZ of welded joints is the primary requirement for selection or calculation of optimal welding conditions. Experimental methods which yield reliable results are most often employed for evaluation of mechanical properties. Mathematical methods are gaining increasing acceptance for investigations to reduce cost of experimental studies and supplement them.

The cooling time $t_{8/5}$ within a temperature range of 850 – 500 °C has a decisive effect on properties of the HAZ of weldments (some authors give a range of 800 – 500 or 800 – 300 °C, depending upon the type of steel).

The E.O. Paton Electric Welding Institute developed a package of applied software for computation of thermal processes occurring in welding, based on solutions of the equations of thermal conductivity [1]. This work was continued in deve-lopment of the «Thermo CCT» software package (Figure 1). Since the 1990s the «Thermo CCT» package has been successfully used at the Urals Polytechnical University (Ekaterinburg, Russia), the Institute for Railway Transport Engineers (Moscow, Russia), the Altai Polytechnical Institute (Barnaul, Russia), as well as at companies «Framatome» (France) and SLV-1 (Germany).

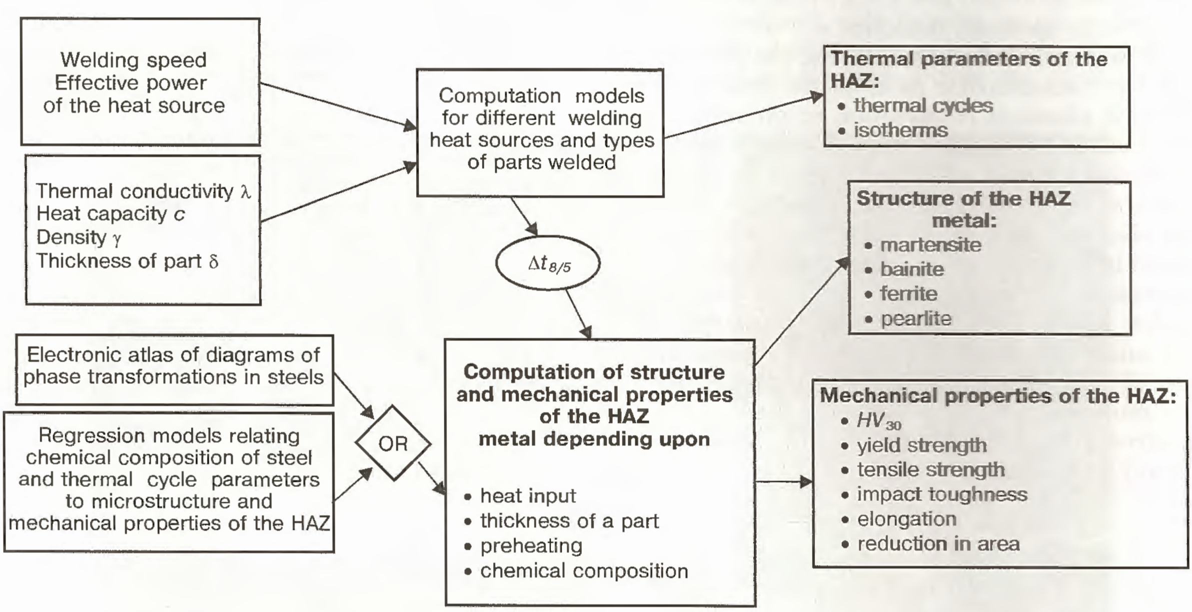

Figure 1. Schematic of the «Thermo CCT» package

Mathematical models for computation of temperature fields

Pictogram	*Model designation*	*Reference*	*Pictogram*	*Model designation*	*Reference*
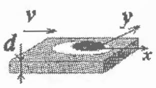	Welding of one homogeneous plate	[5]	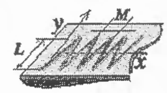	Surfacing of semi-infinite body using heat source with saw-type oscillations	[1]
	Welding of semi-infinite body	[5]	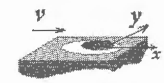	Welding with deep penetration	PWI development
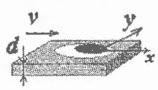	Welding of multilayer plate	[6]	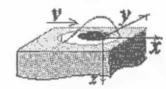	Welding of massive body using Gaussian heat source	Same
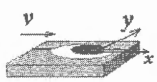	Welding of homogeneous plates of different thickness	[7]	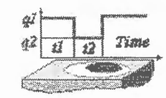	Welding of semi-infinite body using pulse heat source	[4]
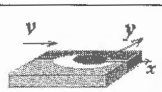	Welding of plates of dissimilar materials	[8]	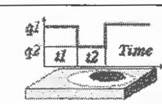	Welding of plate using pulse heat source	[4]
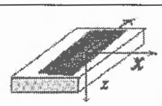	Surfacing of massive body using strip electrode	[1]	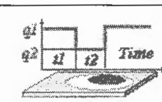	Welding of thin plate using pulse heat source	[4]
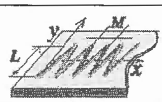	Surfacing of plate using heat source with saw-type oscillations	[1]	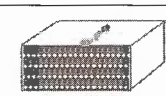	Welding of composite plates	[2, 3]

To simulate thermal processes, the software was supplemented with new modules for computation of temperature fields: welding using pulse modulated power sources and welding of composite material [2 – 4] (Table).

To estimate properties of the HAZ metal, in addition to solving the thermal package problems on the basis of $t_{8/5}$ [4, 6], it is necessary to use atlases of diagrams of anisothermic decomposition of austenite (ADA) and mechanical properties of steels in welding [9, 10] or regression models that relate chemical composition of steel and $t_{8/5}$ to structural and mechanical properties of the HAZ [11 – 13]. They give the following characteristics of metal: phase composition (martensite, bainite, pearlite) and mechanical properties (Vickers hardness HV, tensile strength R_m, yield strength $R_{0.2}$, reduction in area at fracture Z and elongation at fracture A_5). The authors digitized graphical information given in the atlases [9, 10] to give it the form of a data base, further on referred to as the «Electronic Atlas» (EA). EA also contains diagrams of ADA and plots of variations in mechanical properties depending upon $t_{8/5}$. EA includes from the atlas in [9] all steel grades (149 grades) and from [10] only those steel grades for which diagrams of variations in mechanical properties depending upon the cooling rate (90 grades out of 121) are given.

The thermal part of the software (Table) allows computation of thermal cycles at an assigned point (y, z), plotting isothermic lines (following the preliminarily entered list of temperatures) in an assigned cross section xy, yz and xz, as well as rate and time of cooling in an assigned temperature range (including $t_{8/5}$).

The additionally developed software allows computation of the dependence of phase composition or mechanical properties upon the heat input, plate thickness or preheating, based on $t_{8/5}$ obtained from solution of thermal problems for a steel grade taken from EA.

The atlases [9, 10] include steel grades with an assigned chemical composition. However, there is another approach, i.e. prediction of properties from chemical composition of steel. For this, two regression models [11 – 13] are included into the software package, in addition to the atlases. The models enable prediction of variations in phase composition and mechanical properties depending upon $t_{8/5}$ for a selected chemical composition of steel. Besides, the software makes it possible to plot a diagram of dependence of phase composition and mechanical properties upon variations in chemical composition.

In [11, 12] the authors developed regression models for steel of the following chemical composition, %: C $\leq$ 0.4, Mn $\leq$ 2, Si $\leq$ 0.8, Cr $\leq$ 2,

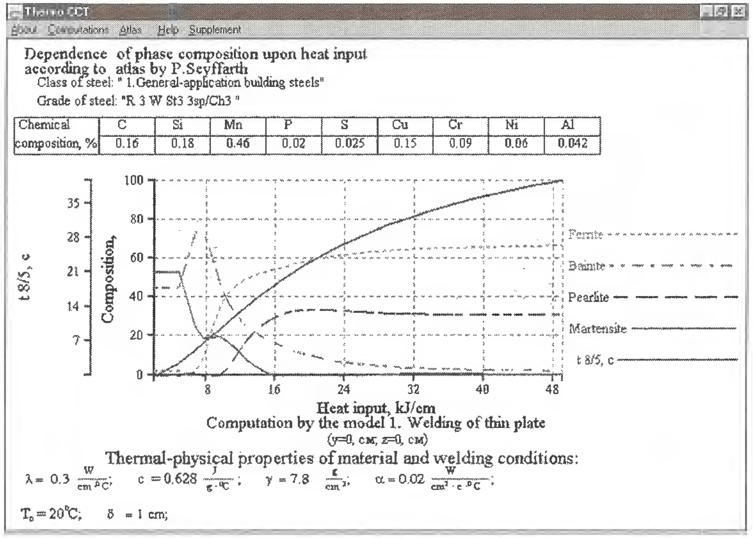

Figure 2.

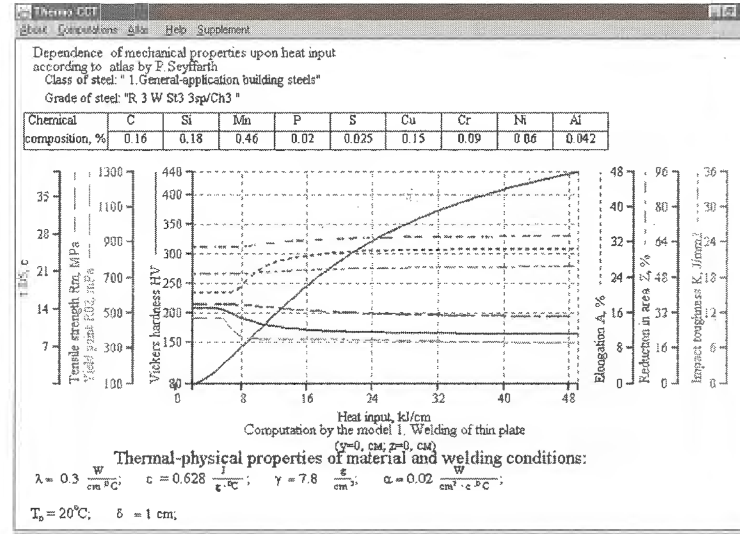

Figure 3.

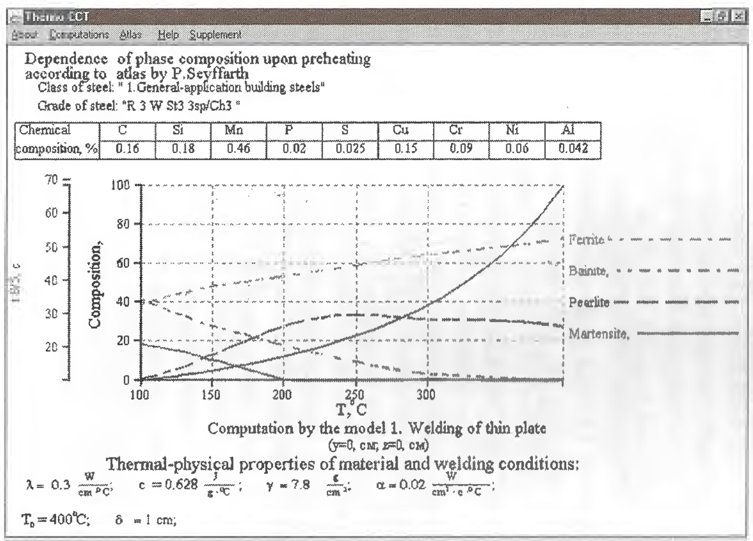

Figure 4.

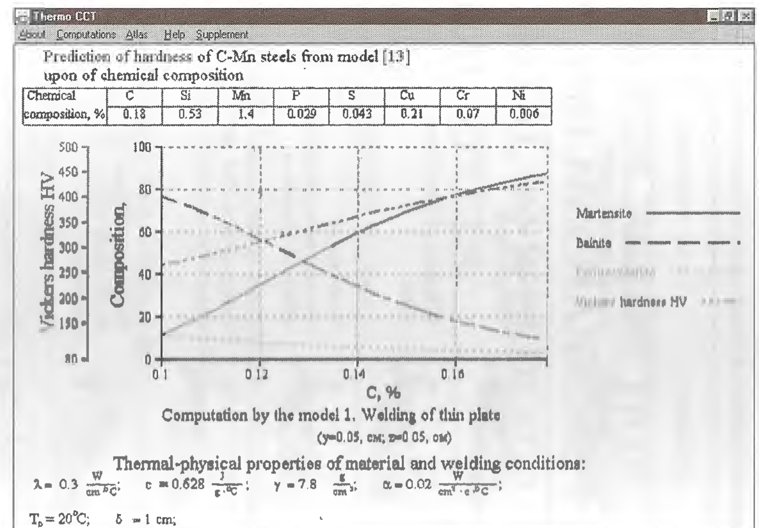

Figure 5.

$Mo \leq 1, Ni \leq 1.5, V \leq 0.3, Ti \leq 0.06, Al \leq 0.066, Nb \leq 0.1, W \leq 0.5, Cu \leq 0.5$, while regression models developed in [13] are designed for steel of the following chemical composition, %: C — 0.10 – 0.13, Si — 0.01 – 0.53, Mn — 0.41 – 1.40, P — 0.080 – 0.029, S — 0.007 – 0.043, Cr — 0.02 – 0.07, Ni — 0.02 – 0.06, Cu — 0.06 – 0.21.

Examples of computation of phase composition and mechanical properties from the atlas by P. Seyffarth are given in Figures 2 – 5.

Therefore, the software suggested enables computation of thermal conditions which ensure mechanical properties of a welded joint within the assigned ranges. It can be used to advantage to assign conditions for welding structural steels for production or training purposes. In addition, the software has an open structure, i.e. at the request of a customer it can be replenished with new models of thermal processes occurring in welding, extra diagrams of decomposition of austenite and regression models of variations in mechanical properties depending upon $t_{8/5}$ for a selected chemical composition of steel.

REFERENCES

1. Abdullakh, V.M., Velicoivanenko, E.A., Demchenko, V.F. *et al.* (1983) *Software package for computation of temperature and concentration fields in welding and surfacing*. Kyiv: PWI.
2. Makhnenko, V.I., Vakulenko, S.A., Demchenko, V.F. *et al.* (1986) Computation of thermal processes in welding of composite materials. *Avtomaticheskaya Svarka*, **9**, 1 – 7.
3. Demchenko, V.F., Vakulenko, S.A. (1986) Computation of thermal processes in welding of a homogeneous plate to composite material. *Fizika i Khimiya Obrabotki Materialov*, **6**, 103 – 107.
4. Muzhichenko, A.F., Demchenko, V.F., Romanenko, A.V. (1991) Software for personal computers for computation of thermal processes in welding and surfacing. *Avtomaticheskaya Svarka*, **6**, 73 – 74.
5. Rykalin, N.N. (1951) *Computation of thermal processes in welding*. Moscow: Mashgiz.
6. Sherstyuk, V.N., Makhnenko, V.I. (1973) Procedure for calculation of optimal conditions for welding ship hull without removal of internal insulation. *Avtomaticheskaya Svarka*, **4**, 74 – 75.
7. Baikova, I.P., Lebedev, A.I. (1960) Effect of a limited width of plate on distribution of temperatures in single-pass arc welding. *Svarochnoye Proizvodstvo*, **5**, 17 – 22.
8. Makhnenko, V.I. (1967) Calculation of thermal pro-cesses in butt welding of dissimilar plates. *Fizika i Khimiya Obrabotki Materialov*, **6**, 78 – 82.
9. Seyffarth, P. (1982) *Grosser Atlas Schweiss ZTU-Schaubilder*. Dusseldorf: VEB-Verlag Technik.
10. Shorshorov, M.Kh., Belov, V.V. (1977) *Phase transformations and variations in properties of steel during welding*. Atlas. Moscow: Nauka.
11. Kasatkin, O.G., Seyffarth, P. (1983) Regression models for estimation of phase composition of the heat-affected zone in welding low-alloy steels. In: *Proc. of II Symp. COMECON*. Sofia.
12. Kasatkin, O.G., Seyffarth, P. (1983) Models for estimation of mechanical properties of the heat-affected zone in welding low-alloy steels. *Ibid*.
13. Ion, J.C., Salminen, A.S., Sun, Z. (1996) Process diagrams for laser beam welding of carbon manganese steels. *Welding Research Supplement*, **7**, 225 – 232.

DISCRETE-TIME CONTROL OF WELDING CURRENT IN POWER SOURCES OF LC TYPE

A.E. KOROTYNSKY
The E.O. Paton Electric Welding Institute, NASU, Kyiv, Ukraine

ABSTRACT

Device with a discrete-time controller of welding current, based on thyristor-semistor commutator, is described. It is shown that its application in the secondary circuit makes the schematic diagram of the LC type power source much simplier. Results of technological tests of this device in welding using the rutile stick electrodes are given.

Key words: *arc welding, resonance welding machine, discrete-time control, resonance of voltages, series oscillatory circuit, transition process.*

Conditions of operation of welding power sources of LC type [1 – 3], close to the resonance of voltages, are adjusted usually by a switching of turns in the welding transformer (TW) primary winding. Sometimes, a switching of elements of a capacity reactor is used for their changing, but in this case it is difficult to provide a stable arc burning within the wide range of welding currents. The mentioned drawback can be eliminated by using additional inductance coils in the power source composition which are capable to provide a matching switching of LC elements. But this complicates the welding machine and, thus, decreases greatly its competitiveness.

We made an attempt to design a rather simple and cheap resonance welding source (RWS), characterized by a high stability of arc burning within the wide range of welding currents. Idea, put into the basis of operation of the suggested RWS is as follows. If to interrupt the voltage, acted at the input of a series circuit of LC during interval t_o, for a time t_p, then its average value will be equal to

$$U_{av} = U_0\,[t_o/(t_o + t_p)], \qquad (1)$$

where U_0 is the effective voltage in circuit; t_o, t_p are the duration of operating cycle and pause, respectively. Let us select the duration of the operating cycle and pause to be equal to an integral number of periods T_m of supply mains: $t_o = nT_m$, $t_p = mT_m$, where n and m are the number of operating and pause periods, respectively. Taking into account these designations the formula (1) can be presented in the form of

$$U_{av} = U_0\,[n/(n + m)]. \qquad (2)$$

Consequently, the relative change of output voltage δU of the device will be equal to

$$\delta U = n/(n + m). \qquad (3)$$

In accordance with an expression (3) the adjustment of the output voltage of the welding machine can be performed by changing parameters n and m. As an example an adjustment characteristic at $n = 10$ is given in Figure 1.

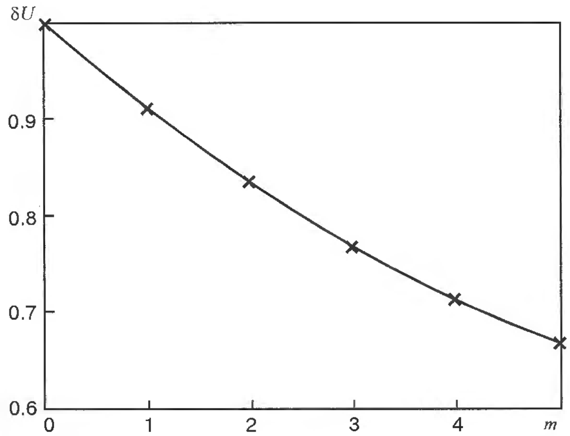

Figure 1. Relation δU (m) at constant amount (n = 10) of operating cycles

The hardware realization of the approach described, using the method of a discrete-time control (DTC) of welding current is accomplished using a scheme shown in Figure 2, *a*. Here, an electron key, made either on two opposite-connected thyristors or on a semistor, is connected in series to a capacity reactor C_r. Operation conditions of the key is determined by a control unit (CU). The latter is synchronized with signals of a former of pulses of a period (FPP), whose input is connected to the mains. This allows switching of voltage at a series resonance circuit, the equivalent scheme of which is given in Figure 2, *b*, just at the moments of its transition through «zero» that greatly simplifies the protection of key elements.

As the practical realization of the DTC method is always associated with a switching of energy-consuming reactive elements of the electric circuit,

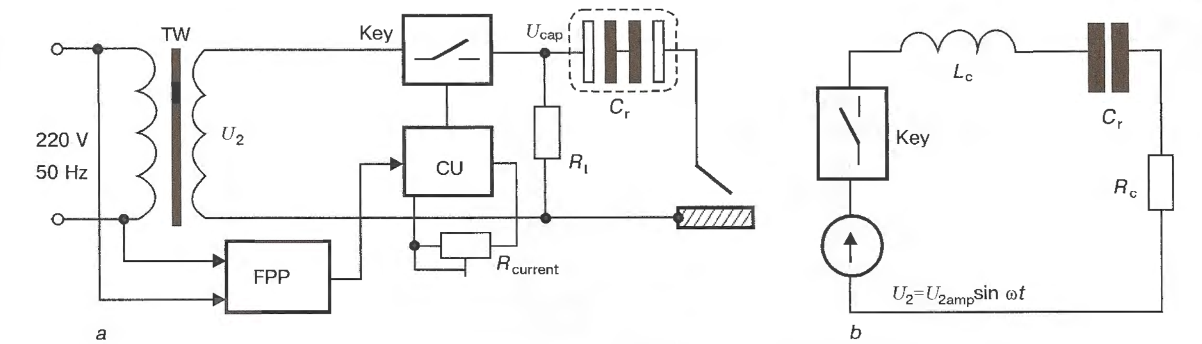

Figure 2. Power source with DTC in secondary circuit (*a*) and its equivalent scheme (*b*)

then it is worthy to analyze the transition processes in the described scheme of the welding machine. As an example we shall determine the duration of a transition process for a series circuit (Figure 2, *b*), whose natural resonance frequency is close to that of the mains ($\omega_c = \omega_m$).

Example. Usually, when calculating RWS a value of electrical capacitance of a reactor C_r is preset equal to 10000 μF, for example, for a limiting current 150 A. The inductance of circuit L_c which will provide the resonance at 50 Hz frequency will be found from formula $L_c = 1/\omega_c^2 C_r = 1/4\pi^2 f^2 C_r$. For the given version we shall obtain $L_c = 1.01 \cdot 10^{-3}$ H. Hence, we shall determine a wave resistance of the circuit $\rho = (L_c/C_r)^{0.5} = 0.318$ Ohm. As a rule, Q-factor of the welding circuit is low and in real devices its value does not exceed unity, i.e. $Q = 1$. Consequently, the circuit resistance determined by formula $R_c = \rho/Q$, will be equal to 0.318 Ohm. Then, the constant of time of circuit τ_c representing relation $2L_c/R_c$ [4] will be 3.2 ms. It is known that the duration of setting the transition process with an accuracy up to 95 % takes place during $3\tau_c$. This means that the preset condition commences during time t_{set} which is lower than the half-period of the mains ($t_{set} = 9.6$ ms).

The illustrated example of calculation of the transition period using DTC method shows that no technical difficulties are expected with switching voltages in the welding circuit. As is follows from the description of the device operation, when this method of control is used, the arc welding conditions are realized with a pulse-time modulation of the welding current. By this reason, when DTC is used, the device should be characterized by a high level of welding-technological properties [5]. As a full extinguishing of the welding arc takes place during time modulation in the pause process, the power source should provide a stable repeated ignition of the arc that is fully typical of the devices of a resonance type, as is known from [6].

Diagrams which correspond to the electrical processes in the scheme shown in Figure 2, *a*, are presented in Figure 3. At each transition of a voltage curve U_2 through «zero» the signals are formed with the help of a differentiating device, whose temporary position denotes precisely an integral amount of periods of the supply voltage. Then, these pulses are fed to a CU selector which determines the duration of the operating cycle n and pause m. At the moments, which correspond to pauses, a blanking signal is fed to the key and an integral number of periods is eliminated from a continuous sequence U_2. This results in action of voltage U_{cap}, shown in the last diagram, in the circuit. For interval t_j ($n = 6$; $m = 3$) $\delta U = 0.67$, while for interval t_{j+1} ($n = 7$; $m = 2$) $\delta U = 0.78$. Selector is made in such a way that parameter n is set preliminary and not changed during welding. Parameter m is preset by a potentiometer $R_{current}$, with the help of which the welding current is determined. Using diagram for U_{cap} we shall determine the frequency of modulation F_{mod} of the welding current by the following relation:

$$F_{mod} = 1/(n + m)T_m. \tag{4}$$

Thus, in our concrete case the frequency of modulation will be constant and equal to 5.55 Hz.

Experience of work with the welding unit of the given type shows that good results can be attained by using a combined scheme of control, i.e. by switching turns in the primary winding and by DTC scheme in the secondary winding. In principle, this control is discrete, but with a small pitch that provides effect which is close to a smooth adjustment of the welding current.

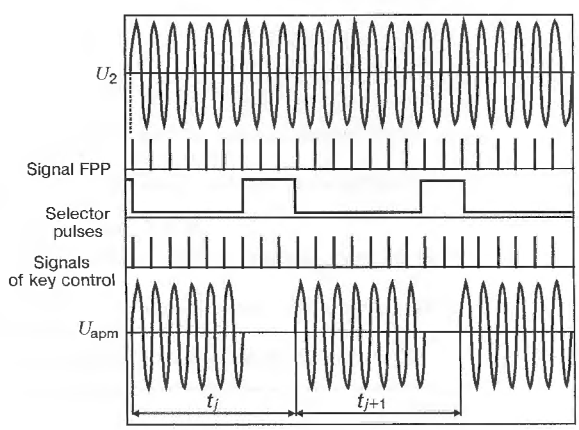

Figure 3. Time diagrams of DTC operation

Table 1

m	δU	F_{mod}	U_m (36 V)	U_m (40 V)
0	1	–	36.0	40.0
1	0.909	4.54	32.7	36.4
2	0.833	4.17	30.0	33.3
3	0.764	3.85	27.7	30.8
4	0.714	3.57	25.7	28.6
5	0.667	3.33	24.0	26.7

Table 1 gives the calculated data of parameters of PWS with a combined scheme of welding current at which the open-circuit voltage has two values (36 and 40 V). The DTC conditions are realized at $n = 10$ and $m = 1 - 5$. Mean value of voltage acting at the output of the power source is determined by formula (2). Here, the modulation frequency depends on the condition selected and increases with the welding current increase. The ranges of F_{mod} change are 3.33 – 4.54 Hz, i.e. not more than 36 %, and the depth of modulation is constant and equal to 100 %. At $m = 0$ the modulation disappears and power sources is transferred to the condition of a continuous current of welding.

Results of testing the designed welding machine with DTC are given in Table 2. During tests the electrodes of ANO-4 (d = 3 or 4 mm) and ANO-21 (d = 2.0; 2.5 mm) grades and electrodes (d = = 1.5 mm) of «Böhler Welding» company were used. As is follows from this Table, 12 versions of external characteristic (EC) are realized in the machine. Thus, it is possible to obtain any value of welding current in the range of 30 – 155 A.

The described scheme of control can be used also in the primary circuit. The scheme is not changed in principle, it should be only added with a unit which prevents the magnetizing of the magnetic core of the welding transformer in case of appearance of a voltage asymmetry at the primary winding, caused by errors of switching, and the snubber of the key should be made more carefully.

Table 2

No. of EC	U_m, V	d, mm	I, A
1	24.0	–	–
2	25.7	1.5	30 – 38
3	26.7	1.5	35 – 45
4	27.7	2.0	40 – 50
5	28.6	2.0	45 – 60
6	30.0	2.5	50 – 70
7	30.8	2.5	65 – 90
8	32.7	3.0	85 – 110
9	33.3	3.0	100 – 120
10	36.0	4.0	115 – 125
11	36.4	4.0	120 – 140
12	40.0	4.0	130 – 155

REFERENCES

1. Lebedev, V.K., Narushkyavicyus, I.R. (1971) Stability of AC arc burning in a circuit with a capacitor. *Avtomaticheskaya Svarka*, **4**, 3 – 5.
2. Lebedev, V.K., Korotynsky, A.E. (1994) AC arc in a circuit with series connected inductor and capacitor. *Ibid.*, **12**, 47 – 48.
3. Lebedev, W.K., Korotynski, A.E., Zuk, G.W. (1997) O niektorych wlasnosciach procesu spawania lukowego z wykorzystaniem zrodel zasilania z obwodem rezonansowym LC. *Biuletyn Institutu Spawalnictwa*, **3**, 34 – 36.
4. Belotserkovsky, G.B. (1969) *Fundamentals of radio engineering*. Moscow: Sov. Radio.
5. Lebedev, V.K., Troitsky, V.A., Belyi, N.G. *et al. Power source for welding with aternating modulated current.* USSR author's certificate **639671**, Int. Cl. B 23 K 9/00. Publ. 03.04.78.
6. Lebedev, V.K. (1996) Peculiarities of power source for arc welding with a capacitor in the secondary circuit. *Avtomaticheskaya Svarka*, **11**, 11 – 14.

FLUX-CORED WIRES FOR SURFACING

A.P. ZHUDRA and **G.A. KIRILYUK**
The E.O. Paton Electric Welding Institute, NASU, Kyiv, Ukraine

Reconditioning or hardening by surfacing can provide an extension of life of wearing parts and their cost-effective repair.

Flux-cored wire has the largest share among other consumables used for these purposes. Such a wire meets all requirements in terms of producing the high-quality metal with preset properties, and it provides an increased deposition efficiency using a comparatively simple equipment under field and factory conditions. Compositions of the deposited

Flux-cored wires for surfacing

Wire grade (designation), diameter, mm	*Hardness of deposited metal, HRC*	*Object treated*
ПП-Нп-30Х5Г2СМ-С (ПП-АН122) 2.2, 2.6	50 – 56	Rollers and rolls of caterpillar machines, chambers and screws of rubber mixers, press tools
ПП-Нп-30Х4Г2М-С (ПП-АН128) 1.8, 2.0	42 – 48	Shaft spiders, dies and presses for hot metal, mounting faces of shafts
ПП-Нп-25Х5МФС-С (ПП-АН130) 2.0, 2.6	46 – 52	Knives, presses and dies, profiled rolls for hot metal
ПП-Нп-30Х4В9Н3Ф-С 2.0, 2.6	50 – 54	Tools and dies for hot pressing of non-ferrous metals
ПП-Нп-25Х5ФМС-Ф 3.6, 4.0, 6.0	46 – 52	Rolls of finishing stands of hot rolling mills, dies Flux АН-20, АН-26
ПП-Нп-35В9Х3СФ-Ф (ПП-3Х2В8) 3.6, 4.0, 6.0	48 – 54	Rolls for hot rolling of pipes and bars, brake pulleys Flux АН-20, АН-26
ПП-Нп-45В9Х3СФ-Ф (ПП-4Х2В8) 3.6, 4.0, 6.0	48 – 55	Same
ПП-Нп-30Х4В2М2ФС-Ф (ПП-АН132) 3.0, 4.0, 5.0	48 – 52	»
ПП-Нп-10Х17Н9С5ГТ-Ф (ПП-АН133) 2.8, 3.6	30 – 35	Sealing surfaces of power and chemical engineering fixture Flux АН-20, АН-28
ПП-Нп-15Х13В2Г2Н2-У (ПП-АН134Г) 2.0, 2.2, 2.4, 2.6	40 – 48	Engine pistons, drilling rig parts resistant to corrosion and gas erosion Flux АН-26, АН-46
ПП-Нп-10Х12М2Н3С-Ф (ПП-АН163) 1.6, 2.0, 2.2	35 – 40	Ship propeller shafts, rudder pintles, press plungers and rods Flux АН-20, АН-26
ПП-Нп-200Х15С1ГРТ-С (ПП-АН125) 2.8, 3.0, 3.2	50 – 56	Excavating machine teeth, bucket noses and ladle walls, grader and bulldozer knives, screen grate bars
ПП-Нп-350Х25Т-С 2.8, 3.2	52 – 58	Same
ПП-Нп-250Х10Б8Т2-С (ПП-АН135) 2.8, 3.2	50 – 58	Suspended tools of bulldozers, ladles of rock excavating machines, blast furnace valves
ПП-Нп-80Х20Р3Т-С (ПП-АН170) 3.0, 3.2	58 – 67	Wheels and scrolls of dredge pumps, dressing and soil-cultivating machine tools
ПП-Нп-150Х15Р3Н3-С (ПП-АН170М) 2.5, 3.0	50 – 58	Same
ПП-Нп-20Х4ГСМФ-Ф 2.0	42 – 46	Steel crankshafts, axles Flux АН-46
ПП-Нп-200ХГР-С (ПП-АН160) 1.6, 1.8	48 – 54	Cast iron crankshafts, casting defects in cast iron
ПП-Нп-18Х1Г1М-Ф (ПП-АН120) 2.0, 3.6	*HB* 320 – 380	Crane wheels, brake pulleys, table rollers, mounting faces of shafts Flux АН-348, АН-46
ПП-Нп-14СТ-С (ПП-АН121) 2.0, 2.8	*HB* 260 – 320	Mounting faces of shafts, casings, parts of railway transport
ПП-Нп-10Х15Н2Т-С (ПП-АН138) 2.2, 2.6	*HB* 240 – 280	Hydraulic turbine chambers and blades, cavitation fracture resistant parts
ПП-Нп-90Г13Н4-С (ПП-АН105) 2.5, 2.8	*HB* 160 – 240	Railway frogs, casting defects in steel G13L

metal are optimized by the comparative full-scale tests, and choice of the surfacing method is based on the required quality of metal deposition.

Self-shielded wire for surfacing, which requires no extra flux or gas shielding of the arc zone, provides the deposition efficiency which is 2 – 4 times higher than in the case of using stick electrodes. It allows saving of surfacing consumables, and in certain cases it presents the only possibility, e.g. in depositing deep internal surfaces.

Wires for submerged-arc surfacing have their own practical application field, as they offer the possibility of producing metal of a consistent preset quality using welding machine tools.

The Table gives grades of the wires which were developed by the E.O. Paton Electric Welding Institute and are now in demand on the market. The trend has been toward increase in demand for small-diameter wires of the well-known grades.

Requirements to technological properties of the wires and ultimate deviations in their diameters, as well as testing rules and manufacturer's guarantees are regulated in GOST 26101 or in specifications for a particular wire grade. According to the standard in force, designation of a wire grade consists of letters ПП (flux-cored wire) and Нп (surfacing); numbers indicate a carbon content (hundredths of a percent), while letters and numbers stand for a content of an element in wt. %. Chemical elements are designated as follows: Х — chromium, В — tungsten, М — molybdenum, Г — manganese, Н — nickel, Б — niobium, Р — boron, С — silicon and Ф — vanadium. Surfacing methods are designated as follows: Ф — submerged-arc surfacing, С — surfacing using no extra shielding, У — submerged-arc, gas-shielded surfacing or surfacing using no extra shielding. The previously accepted wire grades are given in brackets.

For matters associated with purchase of wires, address please:
E.O. Paton Electric Welding Institute
11, Bozhenko Str., Kyiv-150, 03680, Ukraine
Tel.: (380 44) 227 61 57, 220 16 90
Attn.: A.P. Zhudra